AD-A038 014 MAYO FOUNDATION ROCHESTER MINN DEPT OF PHYSIOLOGY AN--ETC F/G 6/19
PROTECTION OF THE CARDIOPULMONARY SYSTEMS AGAINST THE INJURIOUS--ETC(U)
AUG 76 E H WOOD, P A CHEVALIER F44620-71-C-0069
UNCLASSIFIED AFOSR-TR-77-0316 NL

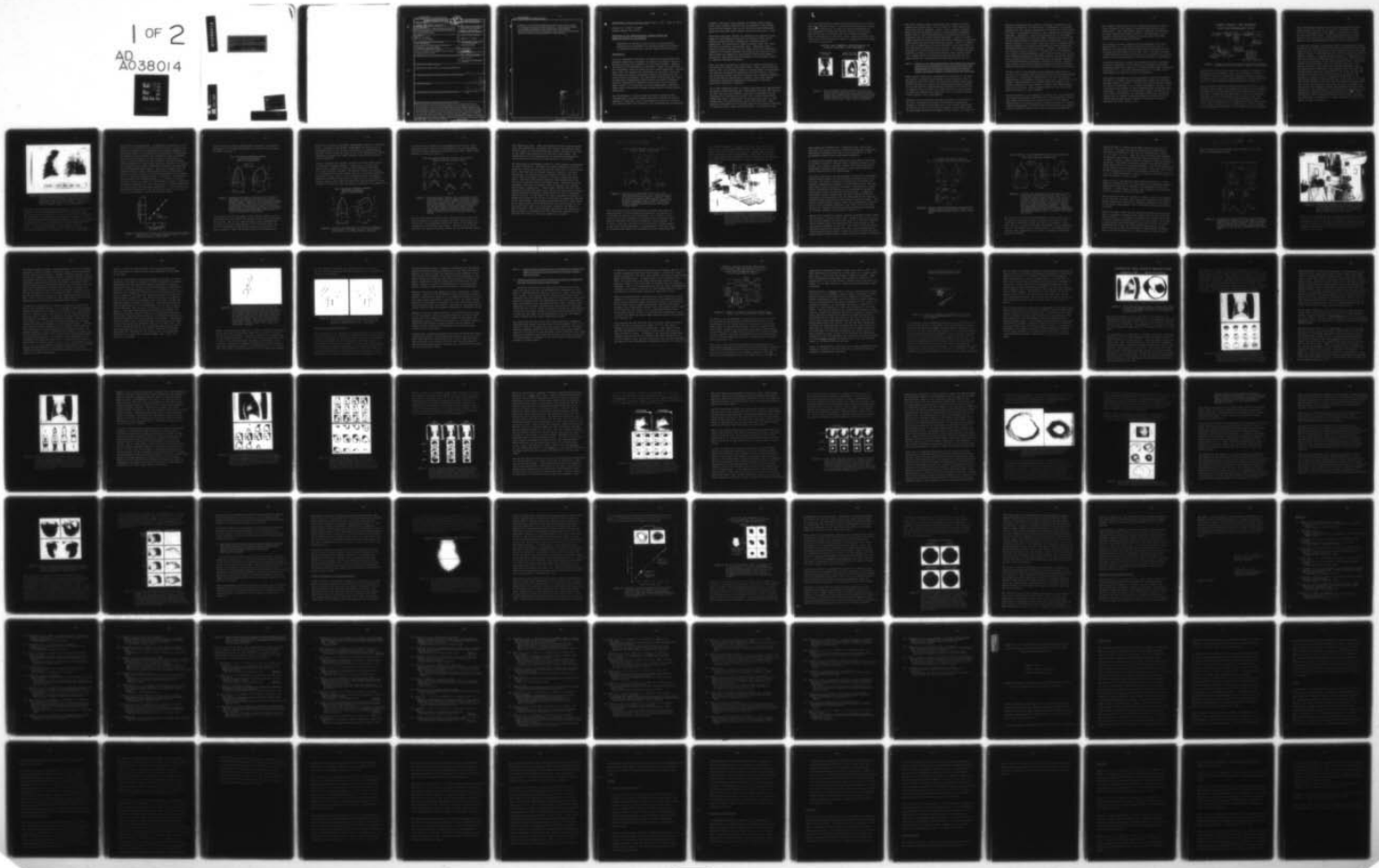

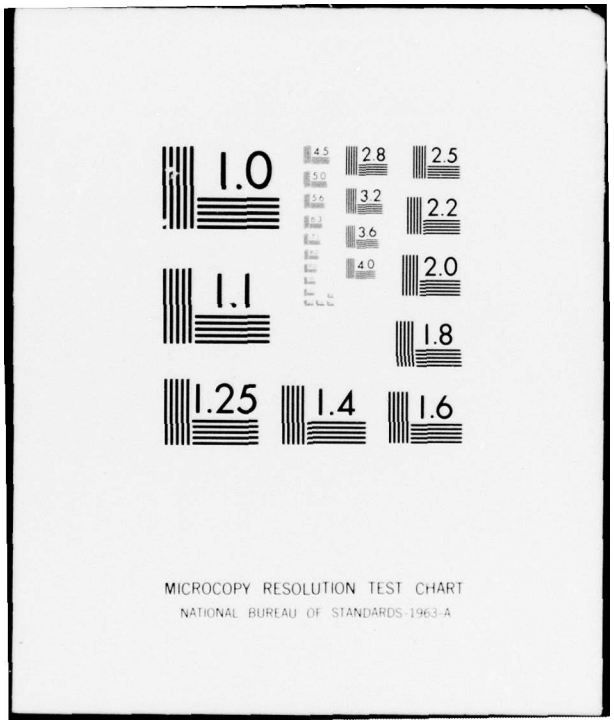
1.0
1.1
1.25
1.4
1.6
1.8
2.0
2.2
2.5
2.8
3.2
3.6
4.0
4.5
5.0
5.6
MICROCOPY RESOLUTION TEST CHART
NATIONAL BUREAU OF STANDARDS-1963-A

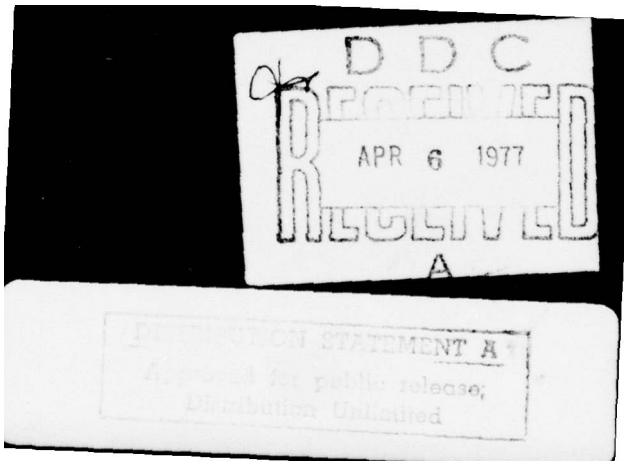
DDC
APR 6 1977
A
DISTRIBUTION STATEMENT A
Approved for public release;
Distribution Unlimited

Unclassified

SECURITY CLASSIFICATION OF THIS PAGE *(When Data Entered)*

REPORT DOCUMENTATION PAGE

READ INSTRUCTIONS BEFORE COMPLETING FORM

1. REPORT NUMBER: AFOSR - TR - 77 - 0316	2. GOVT ACCESSION NO. / 3. RECIPIENT'S CATALOG NUMBER
4. TITLE *(and Subtitle)*: PROTECTION OF THE CARDIOPULMONARY SYSTEM AGAINST THE INJURIOUS EFFECTS OF ACCELERATION	5. TYPE OF REPORT & PERIOD COVERED: Final Scientific Report. 1 Jul 71 - 30 Jun 76.
	6. PERFORMING ORG. REPORT NUMBER
7. AUTHOR(s): Dr. E. H. Wood; Dr. P. A. Chevalier	8. CONTRACT OR GRANT NUMBER(s): F44620-71-C-0069
9. PERFORMING ORGANIZATION NAME AND ADDRESS: Mayo Foundation, Department of Physiology and Biophysics, Rochester, Minnesota 55901	10. PROGRAM ELEMENT, PROJECT, TASK AREA & WORK UNIT NUMBERS: 61102F/9777-02
11. CONTROLLING OFFICE NAME AND ADDRESS: Air Force Office of Scientific Research (NL), Bolling AFB DC 20332	12. REPORT DATE: August 1976
	13. NUMBER OF PAGES: 102
14. MONITORING AGENCY NAME & ADDRESS *(if different from Controlling Office)*	15. SECURITY CLASS. *(of this report)*: Unclassified
	15a. DECLASSIFICATION/DOWNGRADING SCHEDULE

16. DISTRIBUTION STATEMENT *(of this Report)*

Approved for public release; distribution unlimited.

408 960

17. DISTRIBUTION STATEMENT *(of the abstract entered in Block 20, if different from Report)*

DDC
APR 6 1977
A

18. SUPPLEMENTARY NOTES

19. KEY WORDS *(Continue on reverse side if necessary and identify by block number)*

20. ABSTRACT *(Continue on reverse side if necessary and identify by block number)*

The investigators have developed a single source computerized X-ray fluoroscopic system for three-dimensional reconstruction and display of moving organs, particularly the heart, lungs and circulation which provide the potential for studies in intact animals and humans of the dynamic anatomy and associated functions of moving organs in ways never before achievable. For example, these techniques can be used with the subjects in a variety of positions, such as prone, suspine, right and left lateral decubitus, and under

DD FORM 1 JAN 73 1473 EDITION OF 1 NOV 65 IS OBSOLETE

Unclassified

SECURITY CLASSIFICATION OF THIS PAGE *(When Data Entered)*

conditions of increased gravitational-inertial stress such as might be experienced in aerial combat maneuvers. This allows heretofore impossible investigations of the relationships of the dynamic three-dimensional structural geometry to the physical and biochemical functions of both moving and stationary organ systems.

ACCESSION for
NTIS
DDC
UNANNOUNCED
JUSTIFICATION
BY
DISTRIBUTION/AVAILABILITY CODES
Dist. AVAIL. and/or SPECIAL
A

Comprehensive 5-Year Progress Report (July 1, 1971 - June 30, 1976)

Contract No. F44620-71-C-0069
Purchase Request No. 74-007

PROTECTION OF THE CARDIOPULMONARY SYSTEMS AGAINST THE INJURIOUS EFFECTS OF ACCELERATION

Evaluation of effects of time history of gravitational-inertial force environment on regional dynamic distribution of pulmonary ventilation, strains, edema and blood volume.

Introduction

It is of fundamental importance in studies of cardiovascular and pulmonary physiology to measure and analyze the dynamic changes in regional geometry and perfusion in these organ systems. However, the function and performance of the heart, lungs, and circulation are inseparably linked to their motion in three dimensions. Furthermore, since the function and interaction of the heart, lungs and circulation are readily affected by physical interventions into their working environment, and since these interventions may result in functional compensations which obscure the normal functional status or pathological condition of the organ or organ system being studied, it is desirable to devise measurement techniques whose nature involves the minimum possible degree of physiological disturbance.

The transmission of x-rays through the chest produces images (shadowgraphs) with high temporal and spatial resolution without subjective sensations, and is non-invasive in that the x-rays do not directly affect the function of the cardiovascular and pulmonary

Approved for public release;
distribution unlimited.

systems at the dose levels required to produce useful images. Since x-rays readily penetrate and are absorbed to some degree by all bodily tissues, they can be used to produce radiographic images of every body organ ranging in density from bone to lung.

Television techniques provide the capability of recording x-ray images at high temporal resolution in electronic form, which greatly facilitates their transmission, display and more importantly, for quantitative dynamic studies, their very rapid and direct conversion into digital form. High-speed, high-fidelity digital conversion of the images allows the tremendous capability of digital computers for handling the high data rates, data volumes and numbers of calculations required for dynamic analyses of image densities and dimensions to be brought to bear on important biological problems.

Thus, the basic determinants required for accurate estimation of the functional status of the intact heart, lungs, and circulation, namely, their true dynamic changes in regional shape and dimensions, the temporal and regional distribution of blood flow to, within, and from these organs, and their internal and transmural pressures, can be obtained by application of dynamic x-ray video imaging techniques coupled with synchronous recordings of multiple associated physiologic variables.

It is this information that is a basic requirement for understanding the factors which determine man's physiologic response and tolerance to short and long term changes in the force environment such as encountered in conventional aircraft and in manned space flight. Recognizing this, a major effort of our laboratory over the last fifteen years has been directed toward the development, implementation and application of dynamic quantitative imaging techniques to study the heart, lungs, and circulation. In particular, two

unique and complimentary computer-based roentgen-video techniques have been developed (Figure 1) and provide the heretofore lacking technologic capabilities to study the spatial distribution of lung parenchymal stresses and strains, regional lung volumes, regional myocardial perfusion and the true dynamic changes in shape and dimensions of the intact heart, lungs and thorax under normal physiologic conditions, namely, an intact thorax and normal intrathoracic pressures.

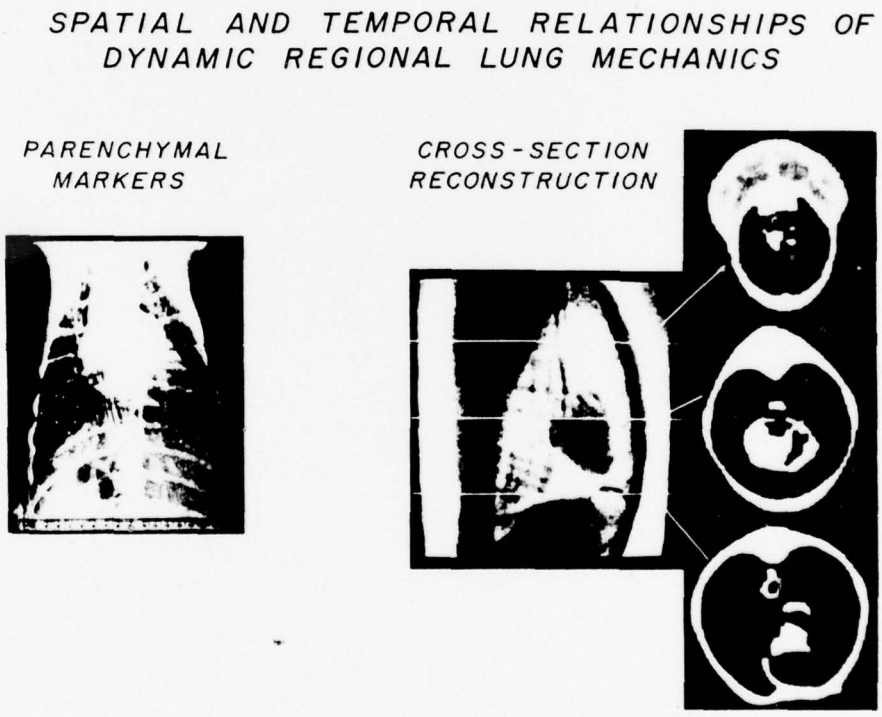

Figure 1 The parenchymal marker technique measures the dynamic spatial distribution of lung parenchymal strains and regional lung volumes while the three-dimensional reconstruction technique measures the dynamic changes in regional shape and dimensions of the heart, lungs, chest wall and diaphragm.

This final progress report for Contract No. F-44620-71-C-0069, covering the period July 1, 1971 to June 30, 1976, consists of three parts and an appendix. Parts I and II contain a comprehensive review and current status of the pulmonary parenchymal marker (Part I) and three-dimensional reconstruction (Part II) techniques and the results derived therefrom. Details of other studies pursued during this period have been documented in published papers and/or previous annual progress reports. Part III consists of a list of publications from our laboratory which were based on work supported by funds from this contract. The Appendix contains a manuscript by Ralph Sturm and co-workers in our laboratory which describes in detail a new state-of-the-art video imaging system (i.e., SSDSR) which was designed by them and was used for the three-dimensional reconstruction studies described in Part II.

PART I: Spatial (i.e., Three-Dimensional) Distribution of Regional Lung Strains and Volumes in the Intact Canine Lung From Measurements of the Dynamic Displacements of Roentgenopaque Parenchymal Markers in Anesthetized and Awake Dogs

Under dynamic conditions, the mechanical properties of the lungs and thorax, including the diaphragm, play an important role in determining the total volume, and the intrapulmonary distribution of the inspired gas reaching the alveolar gas exchange surfaces. It is known that the intrapulmonary distribution of inspired gas is altered by such factors as 1) body position; 2) lung volume; 3) chest wall geometry and compliance; and 4) increased gravitational-inertial force environments.

Because of the very fragile anatomic structure of the lungs and the large intrathoracic pressure differentials generated by changes in the force environment due to the extreme differences in specific gravity of the gaseous contents of the alveoli and the parenchyma and blood surrounding these alveoli, the lungs are

the most susceptible organ system in the body to malfunction and structural injury due to acceleration. Furthermore, it is quite possible that the regional distribution of mechanical stress within the lung is a predisposing factor in the localization of pulmonary pathology. Therefore, a quantitative description of the dynamic spatial distribution of lung parenchymal stresses and strains and the associated changes in dynamic shape and dimensions (i.e., the dynamic geometry) of the intact lungs and thorax is required before further progress can be made in describing the three-dimensional mechanical behavior of the intact lung. However, elucidation of the intrinsic elastic behavior of the lung and its relationship to the chest wall and diaphragm require studies of the intact lung with techniques possessing sufficient temporal and spatial resolution to permit quantitative measurements of the dynamic changes in the three-dimensional parenchymal stresses and strains, regional lung volumes, and thoracic shape and dimensions along with simultaneous measurements of transpulmonary and intravascular pressures.

To date, most of the knowledge of the mechanical properties of the lung in the intact thorax has been derived from pressure-volume curves (i.e., "compliance" measurements)(1,2) and the regional distribution of an inspired radioactive gas (e.g., xenon-133)(1,3,4). However, these methods do not possess sufficient temporal and spatial resolution to allow study of regional lung displacements, strains and volumes. Hence, dynamic studies of the intact lung have, heretofore, not been possible.

We have developed in our laboratory a method (5,6) for determining the spatial and temporal distributions of lung parenchymal strains and volumes within the intact thorax by recording the dynamic displacements of radiopaque metallic markers by means of a biplane videoroentgenographic recording system which permits high temporal (60-per-second) and spatial ($\pm$1.0 mm) resolution measurements of

the "tagged" lungs during various respiratory maneuvers, alterations in posture, and changes in gravitational-inertial force environments. This "parenchymal marker" technique has been used to study regional parenchymal strains in anesthetized, as well as awake, spontaneously breathing dogs and results from these studies to date are summarized below.

The technique involves tagging the lung parenchyma with radiopaque markers (5). The metallic markers, which are 1-mm in diameter, are implanted percutaneously under fluoroscopic control throughout the parenchyma of the right lung of anesthetized dogs. A three-dimensional grid-like array of up to 30 markers is obtained without causing physiologically significant pneumo- or hemothorax.

Postmortem pathologic studies have revealed no pleural adhesions following implantation of the markers and pulmonary parenchymal pathologic changes are limited to a region 100-200 micra surrounding each marker (5). A minimal recovery period of 2-3 weeks is provided before the dogs are used in an experiment.

The dynamic displacements of the parenchymal markers are measured by means of a biplane videoroentgenographic system and recording equipment shown in Figure 2. The two x-ray sources can be arranged in either an orthogonal or in a stereo arrangement as shown. The x-ray sources are pulsed on nearly simultaneously and transradiate the thorax. The respective fluoroscopic images, recorded on two 9-inch image intensifiers, are scanned by television (Plumbicon) cameras and the biplane videoroentgenograms are combined into a single biplane video format (Figure 3) by special electronic switching and delay circuitry (7).

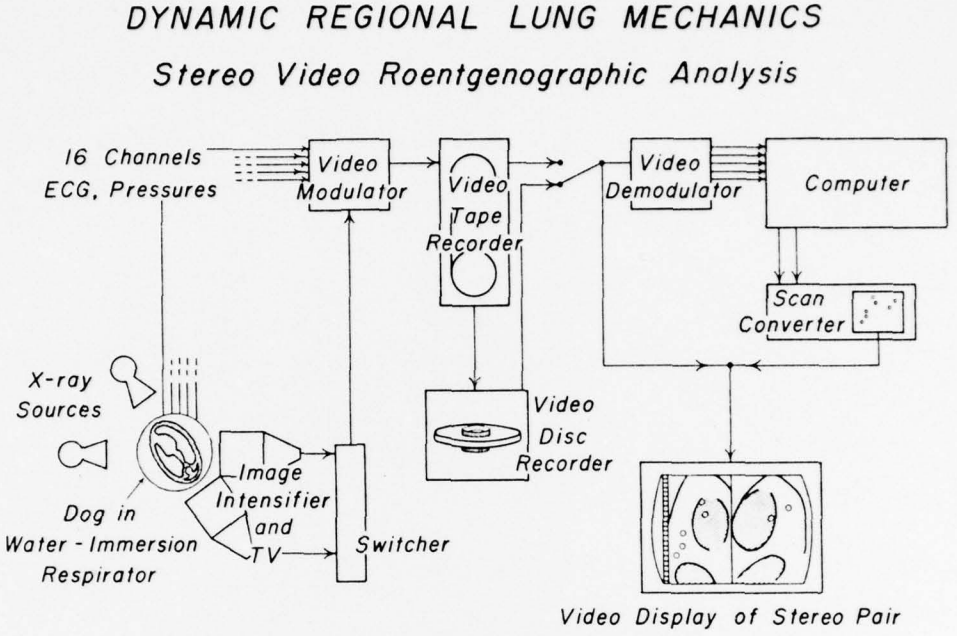

Figure 2 Schematic drawing of biplane videoroentgenographic system used to study dynamic regional lung mechanics.

The sequence of 60/s biplane images are recorded on videotape in absolute temporal synchrony with up to 16 channels of analog information, such as intrathoracic pressure, ECG and ventilation at sampling rates as high as 1000 samples/s per analog channel by means of a video amplitude modulator-demodulator system (8).

Since the image intensifier causes pincushion distortion in the recorded video images, which affects the accuracy of the geometric measurements of the distribution of the metallic markers within the image, a method has been developed to express the magnitude and direction of this distortion over the entire image field covered by the face of the 9-inch image-intensifier screen. A fourth order polynomial with 15 terms relating selected locations in the image to their true, x-y coordinates is used to correct for the pincushion distortion in the recorded x-ray video images.

This predetermined polynomial can correct the geometric distortions (ranging from zero at the center of the field to about 1.5 cm at the periphery of the image) to less than 1 mm error for the entire video field. Image magnification due to divergence of the x-ray beam as it traverses from the finite-size source to the image-intensifier screen is also corrected (5).

To facilitate analysis, the biplane images and multichannel analog recordings are transferred from videotape to stop-action video disc (Ampex DR-10A), and the tracking of the geometric positions of the metallic markers is performed with the aid of an operator-interactive computer program. A computer-generated cursor is displayed on a video scan converter (Tektronix 4501) which "mixes" the cursor with the stop-action display of the biplane thoracic image. The investigator moves this cursor until it coincides with one of the metallic markers in the video image and then depresses a key on the keyboard which indicates to the computer (CDC 3500) that the two-dimensional geometric coordinates of the cursor and thus the metallic marker are to be read and stored in an array. This procedure is repeated until the geometric coordinates of all identifiable markers on both projections of the lungs for a single video frame (1/30th s) are input into the computer, at which time the computer also digitizes and stores the up to 16 channels of analog data that had been recorded simultaneously with the video information. The coordinates of each marker are corrected for pincushion and magnification distortions and then the true three-dimensional spatial coordinates of each marker within the thorax are determined. An example of a video frame used for such a procedure is shown in Figure 3.

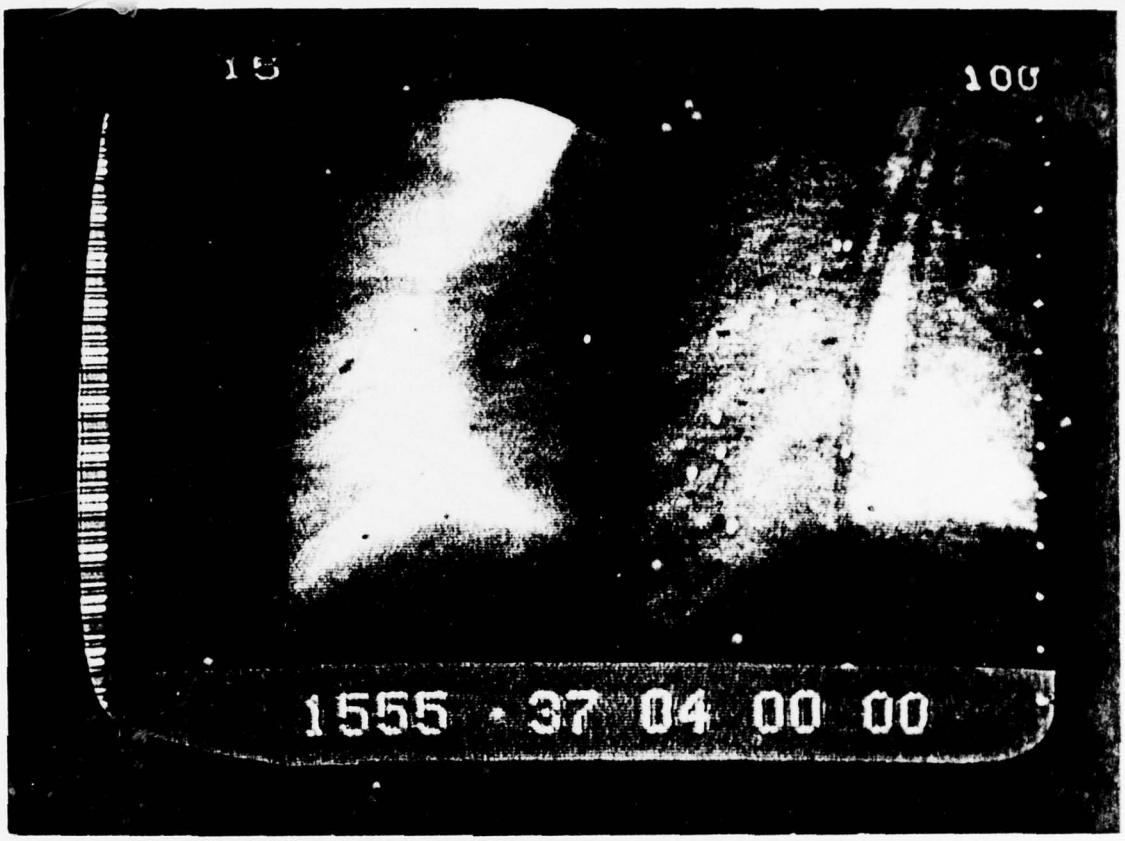

Figure 3 Photograph of single stop-action frame of stereo biplane videoroentgenogram illustrating the stereo biplane view of the canine right lung with metallic parenchymal markers in both images. Computer-generated cursor dots used to input geometric positions of markers shown in right-hand image.

The simultaneously recorded analog information is contained in the "ribbon" at the normally unused left margin of the video image while identification information (e.g., time and code), added during the experiment, is displayed at the bottom of the image. In this particular photograph the geometric positions of the metallic markers at end expiration are indicated by the bright computer-generated (cursor) dots in the right panel of this biplane thoracic image. Following determination of these points, the video disc was stepped forward to end inspiration to show the displacement of

the markers from these points. By comparing the positions of the markers at end expiration as indicated by the white (cursor) dots and at end inspiration as indicated by the markers themselves, a qualitative measure of the direction and magnitude of parenchymal displacement occurring during one respiratory cycle is obtained. The quantitative accuracy of this technique is indicated in Figure 4, which compares the actual measured distances between markers embedded in a Lucite plate which was rotated in the biplane x-ray system and the computer-determined distances obtained from the videoroentgenographic images. This graph indicates that the computer analysis, which removes pincushion and magnification distortion and calibrates the corrected coordinates to real dimensions is accurate to within $\pm$1.0 mm. In addition, calculations of strains between the embedded markers (i.e., strain = 0) during rotation resulted in a mean (N = 294) strain of 0.004% $\pm$ 0.002 (SEM) for markers separated by 1, but not more than 5 cm after correction for magnification and pincushion distortions. In our studies, only marker pairs separated by 1 cm, but not more than 5 cm, are used in calculating dynamic regional parenchymal strains.

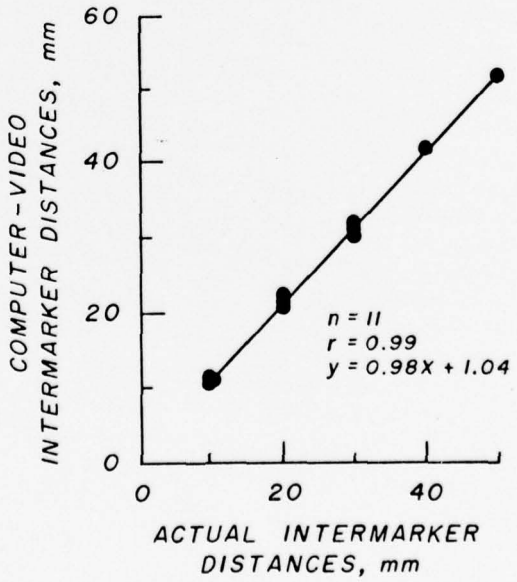

Figure 4 Comparison of actual and computer-calculated distances between pairs of radiopaque markers fixed at known distances within a Lucite plate.

Results from the computer program which calculates the geometric coordinates of the individual markers in three-dimensional space are shown in Figure 5.

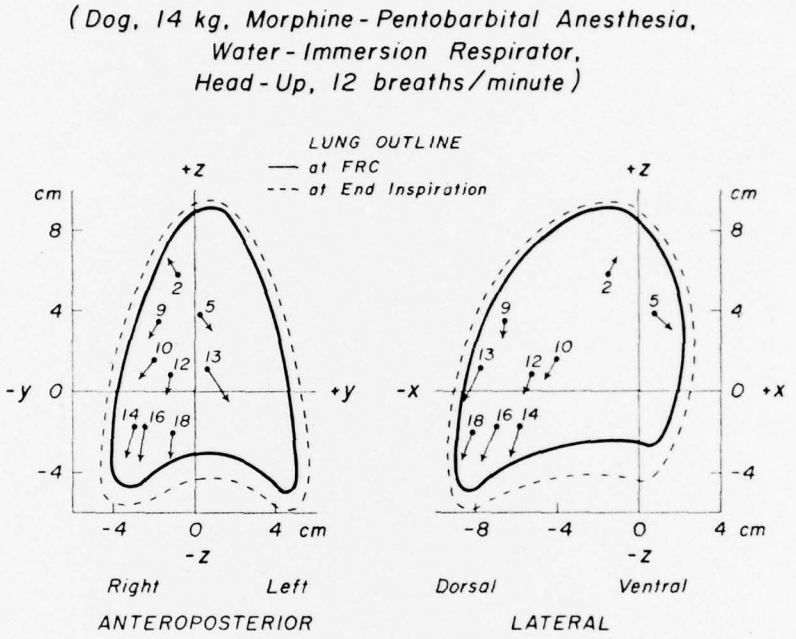

Figure 5 Comparison of regional displacements of metallic parenchymal markers in the right lung during a respiratory cycle starting from functional residual capacity (FRC). Positions of the individual markers at end expiration (FRC) and end inspiration are indicated by the tail and the point of each arrow, respectively. Orientation and length of each arrow denotes direction and magnitude, respectively, of regional parenchymal displacement.

The spatial locus of each marker can be found by looking at the anteroposterior (left panel) and lateral (right panel) projections of the lung. The tail of each individual arrow represents the position of that particular marker at end expiration while the point of each arrow represents the position of the marker at end inspiration. Thus, the arrows indicate the direction and

magnitude of regional parenchymal displacements during a respiratory cycle. Analysis of the dynamic displacements of these metallic parenchymal markers can be used to determine the distribution of regional strains within the lung of the intact thorax during various respiratory maneuvers and under different gravitational-inertial force environments.

Figure 6 indicates the anatomic positions of three "marker-pairs" at functional residual capacity. These pairs of markers were selected for analysis of strain in three regions of the lung, i.e., apex, midlung, and base. The dynamic changes in distance in three-dimensional space between each pair of markers represents the strain ($\Delta L/L_o$, where ΔL is the measured change in distance between two markers at any point in time and L_o is the measured distance between these same two markers at end expiration) in that region of the lung for that particular orientation of the marker pair.

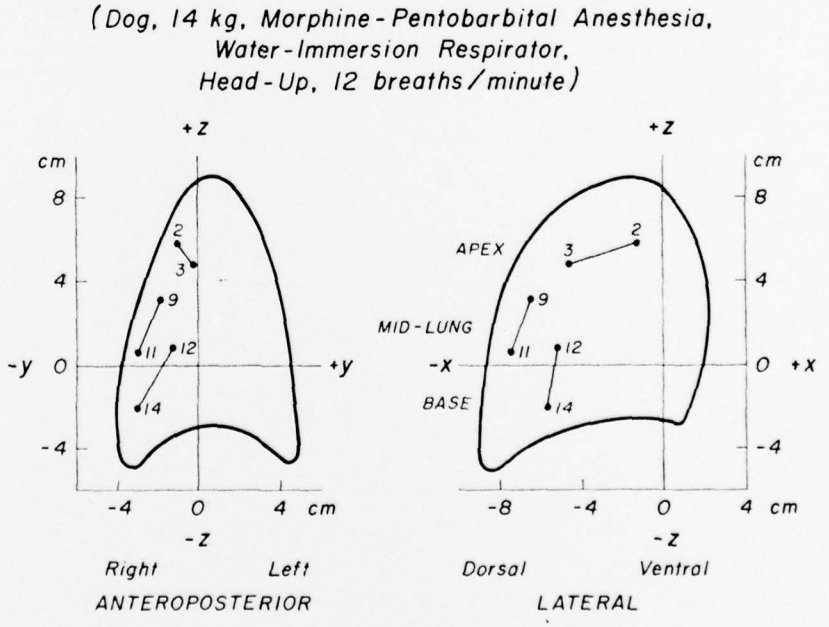

Figure 6 Location and orientation of 3 pairs of markers at FRC selected to measure strain in three regions of the lung, i.e., apex, midlung, and base.

Distributions of regional lung parenchymal strains during three respiratory cycles starting at approximately FRC (closed symbols) and during three respiratory cycles starting at FRC + 200 ml (open symbols) are shown in Figure 7.

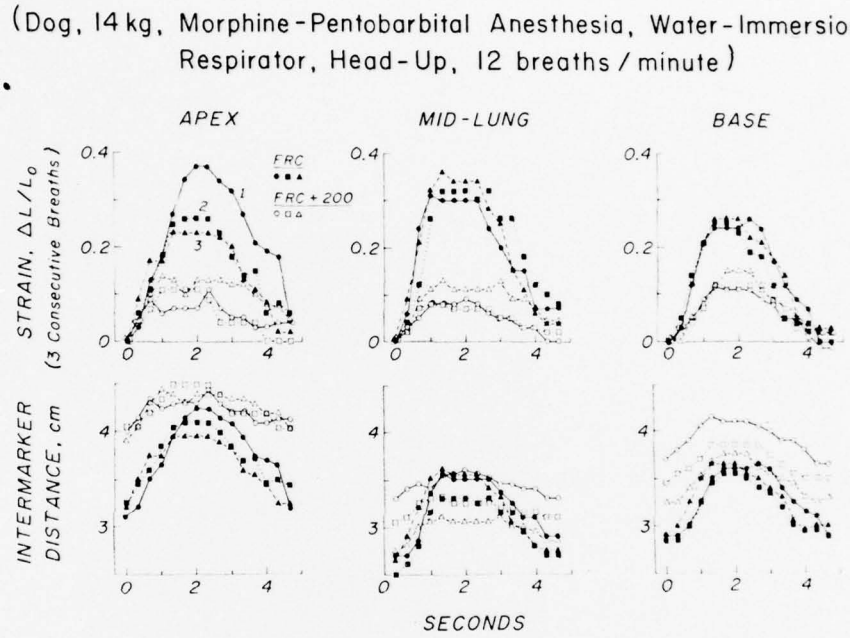

Figure 7 Distributions of regional lung parenchymal strains and displacements during three respiratory cycles starting at FRC (closed symbols) and three respiratory cycles starting at FRC + 200 ml (open symbols). Upper three panels indicate strain distributions for the three pairs of markers shown in Figure 6 in the apex, midlung, and base, respectively. Lower three panels represent absolute distance between marker pairs at the three specified lung levels.

The top three panels indicate strain distributions for the three pairs of beads in the apex, midlung, and base, respectively. It can be seen that parenchymal strain was larger at the lower lung volume than at the higher lung volume. The lower three panels represent the absolute distance between the various markers during

the respiratory cycle. While the absolute distance between marker pairs was increased at the higher lung volume, the absolute excursion or change in intermarker distance during respiration was less at the higher lung volume than at the lower lung volume. The reproducibility of the measurements of regional distributions of strain from cycle to cycle can also be seen in this figure.

The anisotropy of parenchymal strains in three separate lung regions is shown in Figure 8. The upper two panels represent the anteroposterior and the lateral projections of three sets of three markers each. The three sets of markers represent regions in the apex, the midlung, and the base and were chosen to include, for each region, pairs of markers oriented in virtually orthogonal directions. The lower three panels represent the computed strain for the pairs of markers shown in the upper panel. These three panels represent strains for two marker pairs in the apex, the midlung, and the base, respectively. These graphs indicate that for three sequential breaths the marker pairs in both the apex and the midlung regions exhibited different strains relative to their orientation within the lung. In the base of the lung a paradoxical movement is exhibited by beads 15 and 18 where a decrease in separation occurred during inspiration. This behavior has been observed in other parts of the lung as well and was predicted by West and Matthews (9) for the apical region but not for the basal region of the lung of a head-up animal. Thus, this technique may provide the experimental data necessary for evaluation of the theoretical analyses (9) of stresses and strains in the lung caused by its weight.

BEST AVAILABLE COPY

(Dog, 14 kg, Morphine-Pentobarbital, Anesthesia, Water-Immersion Respirator, Head-Up, 12 breaths/minute)

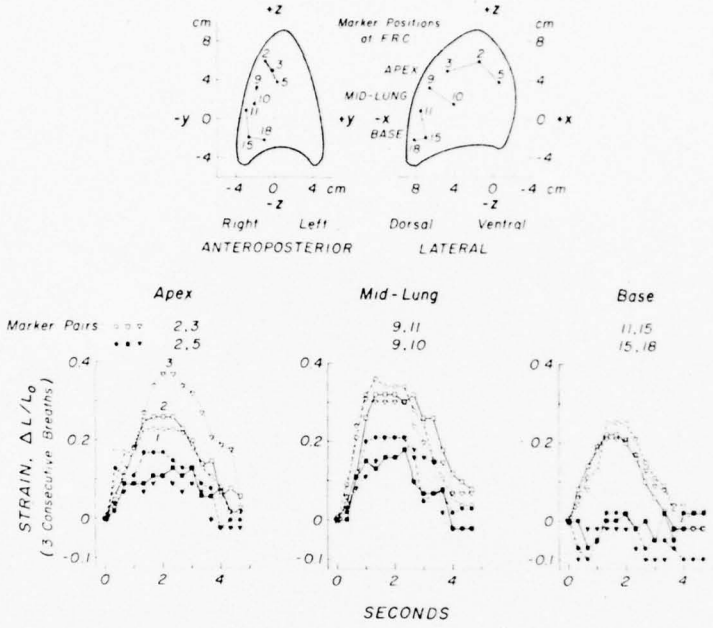

Figure 8 Anisotropy of parenchymal strains in three different regions of the lung. Upper two panels show location of three sets of 3 markers chosen to include in each of three regions (i.e., apex, midlung, and base) pairs of markers oriented in virtually orthogonal directions. Lower three panels represent strains for pairs of markers in upper panel.

Since the above studies were performed on anesthetized dogs supported head-up in a water-immersion respirator, the question as to whether the gravitational orientation (i.e., head-up) of the dogs as well as the presence of a column of water surrounding the animals influenced the results obtained had to be answered. To do this, 6 dogs were selected for training prior to being studied in the awake standing position. The parenchyma of the right lung of these dogs was tagged with radiopaque metallic markers and they

were allowed a minimum of 3 weeks to recover. After this period of time, the animals were brought to the laboratory, on an individual basis, and allowed to run free for a short time to familiarize themselves with the surroundings. They were then placed in a Pavlovian-type sling (Figure 9) and positioned on the fluoroscopic table where they eventually learned to stand quietly for 20-30 minutes.

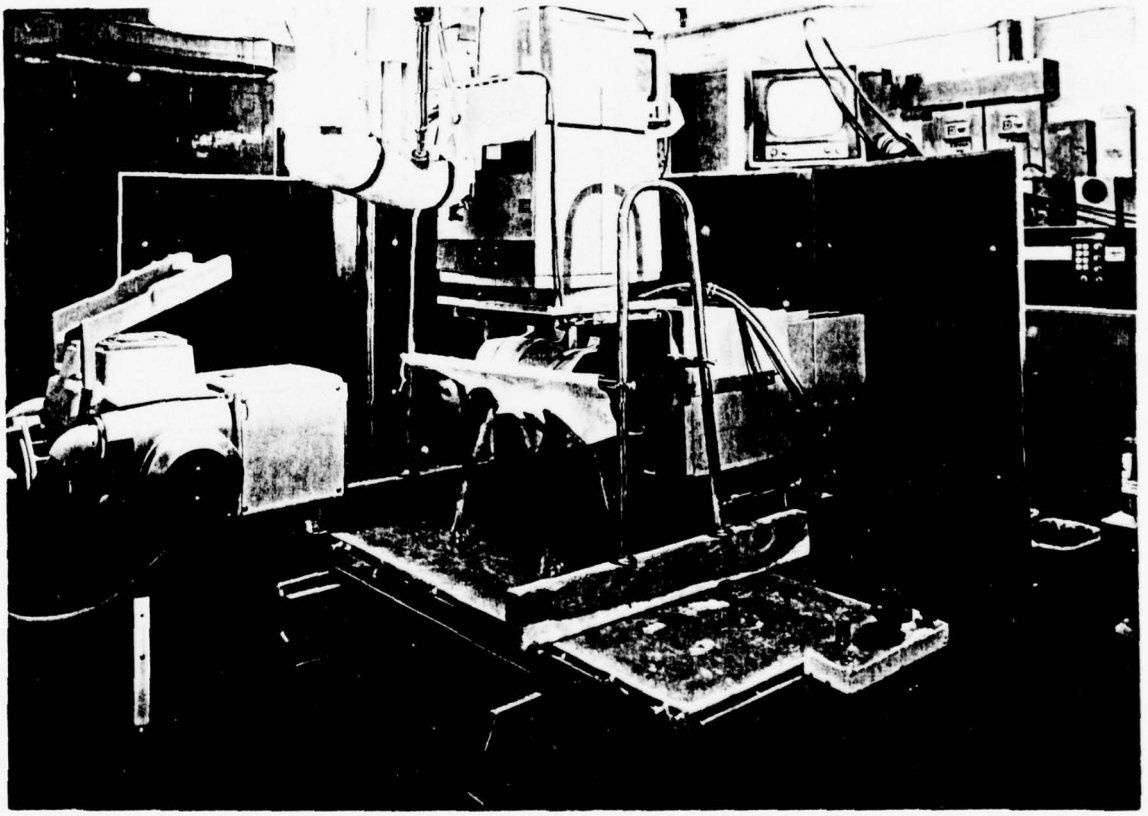

Figure 9 Awake dog standing in a Pavlovian-type sling in front of the biplane videoroentgenographic recording system. Dog can also be anesthetized and supported in this "prone" position to maintain the same orientation of the lung and intrathoracic pressures in the gravitational field as in the awake state.

This regimen was followed for 3 consecutive days, but on the third day, the x-ray units were activated and biplane videoroentgenographic recordings were made of the displacements of the parenchymal markers during spontaneous breathing.

No pressures or volumes were obtained in these awake animals and no attempt was made to influence their breathing pattern or frequency. In 5 of the 6 animals, several 5-10 minute segments of spontaneous breathing were recorded in each animal before the animal moved and had to be repositioned.

Continuous tracking of the displacement of individual parenchymal markers during inspiration and expiration revealed that for the most part the markers returned to the position from which they started, although minor degrees of irreversibility were seen and these were corrected within 2-3 breaths. Occasionally, a reproducible hysteresis was observed in the displacement pathways of some markers during inspirations and expiration. In addition, parenchymal markers located near the heart undergo additional oscillation and displacement due to cardiogenic motion with this movement being particularly visible during expiratory pauses. The extent to which cardiac motion alters the stress-strain relationship of lung parenchyma adjacent to the heart has not yet been determined. Regional lung strains during spontaneous breathing in an awake standing dog are shown in Figure 10.

Markers were selected to measure regional parenchymal strain along the horizontal or Z-axis of the lung. Markers 2,3,7,10 and 12 all lie at approximately the same level, that is on the same isohydrostatic pressure plane and extend over the major portion of the apex-to-base dimension of the lung. Note that the strains between successive marker-pairs along this line are very similar during the two breaths plotted here. During the time of recording, this animal sighed spontaneously and those results are shown in Figure 11.

BEST AVAILABLE COPY

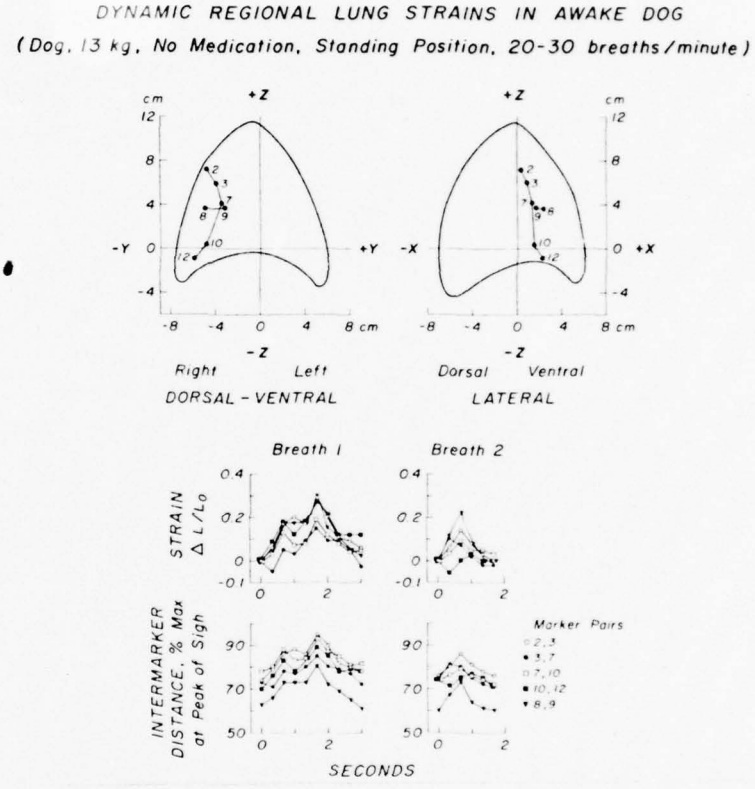

Figure 10 Dynamic regional parenchymal strains between markers lying along horizontal Z-axis (i.e., isohydrostatic pressure plane) of the canine lung.

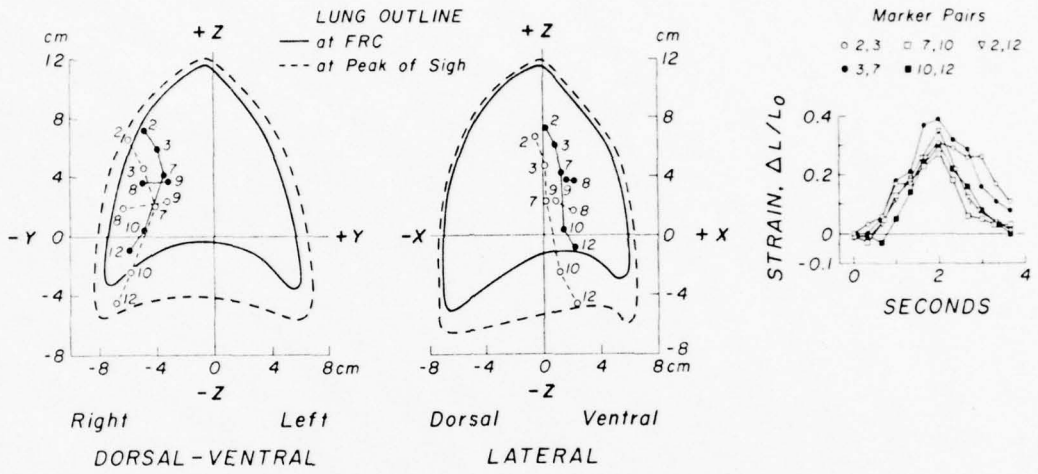

Figure 11 Regional lung parenchymal strains between markers lying along horizontal Z-axis of lung during spontaneous sigh in awake standing dog. Outlines of lung at end-expiration, taken as functional residual capacity (FRC) for this animal and at total lung capacity (TLC) are shown to indicate extent of lung parenchyma displacement during this particular respiratory maneuver. Regional lung parenchymal strains, determined by measuring the dynamic change in distance in three-dimensional space between marker-pairs, is shown in the right-hand panel.

The outlines of the lung at end-expiration, taken as FRC, and at the peak of the sigh are shown to indicate the extent of lung parenchyma displacement during this particular maneuver. Note again the near equality of regional parenchymal strains suggesting that the lung behaves like a linear spring in the isohydrostatic pressure plane regardless of the types of voluntary respiratory maneuver performed.

The anisotropy of regional parenchymal strains can be seen in Figure 12. The upper two panels represent the dorsal-ventral and lateral projections of two sets of 3 markers each; namely, 3, 6 & 7 and 7, 10 & 11. These two sets of markers were selected to represent the midlung and the base and were chosen to include in these 2 regions, pairs of markers oriented in virtually orthogonal directions. The middle two panels represent the strains between these markers during 3 consecutive breaths. Note the reproducibility of the regional strains from cycle to cycle. Note also that strains between marker-pairs oriented in orthogonal directions (e.g., 7, 11 vs 7, 10 (right-hand panel)) differ by 75-80%, with these differences being significant at the 1% level.

Thus, in both 1) anesthetized dogs supported head-up in a water-immersion respirator and in 2) awake dogs in the standing position, significant anisotropy of regional lung parenchymal strains was observed. In other words, regional lung expansion and contraction is not necessarily isotropic or uniform.

This anisotropic behavior reflects, at least in part, the influence of the shape of the lung, local distortion produced by the beating heart, diaphragm and chest wall, regional variation in the degree of structural inhomogeneity, and a non-uniform spatial distribution of stress.

Since it has been shown that the mechanical behavior of the intact lung is dependent on absolute lung volume and the lung's previous volume history, it is necessary to measure lung volume and be able to relate regional mechanical behavior to lung volume. To do this, we have designed and constructed a radiolucent lucite air-filled plethysmograph (Figure 13) which permits quantitation of lung volume and can be used with anesthetized spontaneously breathing dogs in various positions (i.e., prone, supine, right and left

BEST AVAILABLE COPY

lateral decubitus) and with awake dogs trained to lie quietly with the plethysmograph closed.

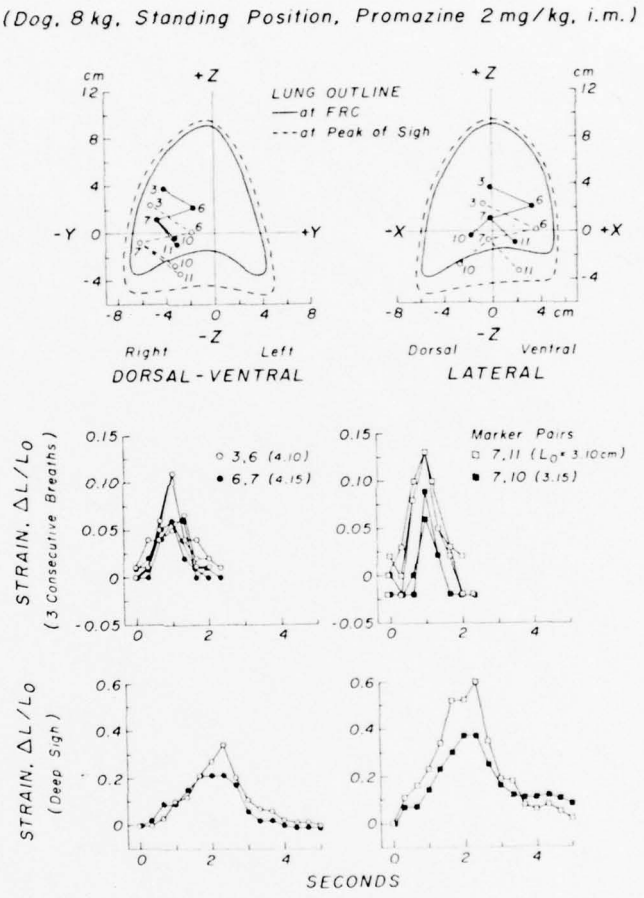

Figure 12 Anisotropy of lung parenchymal strains during spontaneous breathing and a deep sigh in an awake standing dog. Upper two panels show locations of markers selected for analysis. Lower two panels represent strains during spontaneous breathing (middle row) and during a spontaneous sigh (lower row).

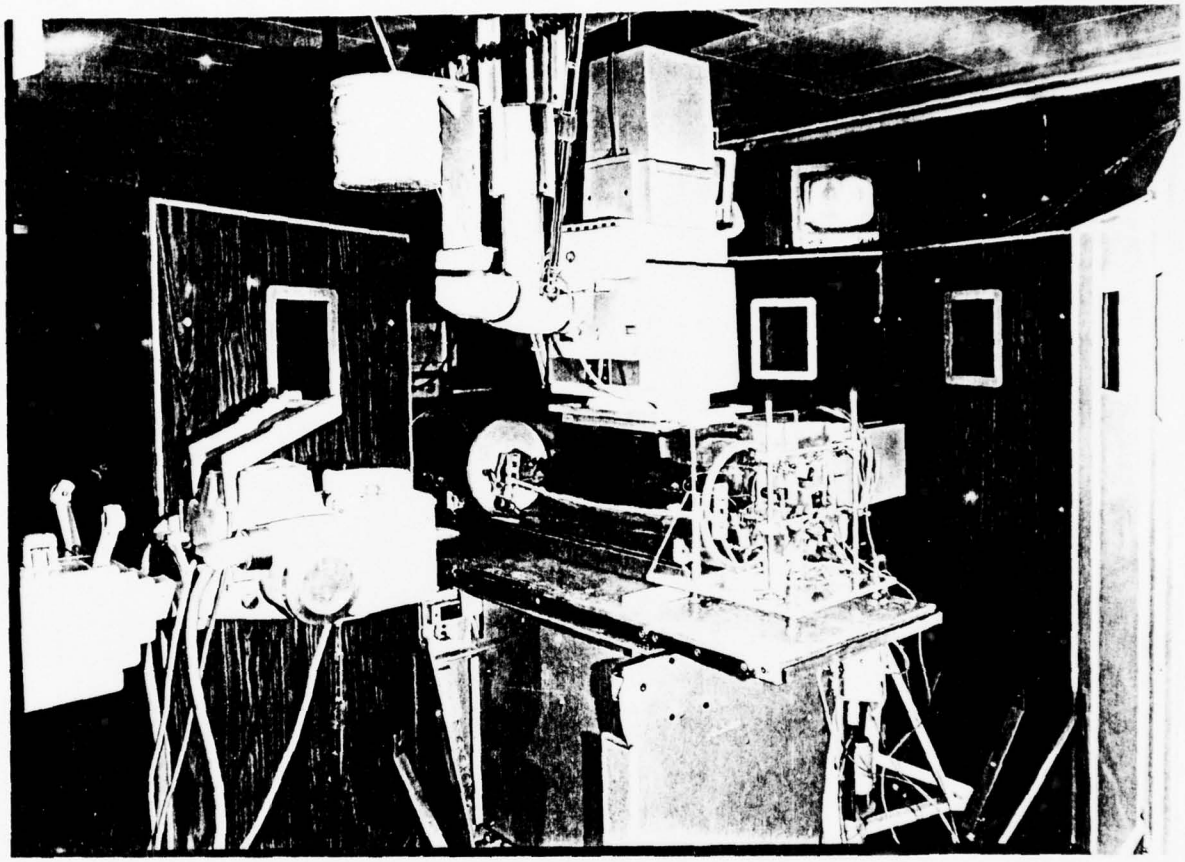

Figure 13 Radiolucent plethysmograph positioned in front of the biplane videoroentgenographic system. An anesthetized dog is shown in the plethysmograph in the prone position. Plethysmograph permits quantitation of lung volume.

Studies with anesthetized dogs in different positions are currently in progress. A measure of the transpulmonary pressure (TPP) or distending pressure of the lung is obtained by subtracting airway pressure from pleural pressure, the latter being provided by the pressure recorded from an esophageal balloon positioned at the mid-lung level (10,11).

The animals breathe through a pneumotachograph in order to measure velocity of flow and volume (integral of flow) of air moved during various respiratory maneuvers. Selected breathing regimens (i.e., various tidal volumes and cycle lengths, including periodic respiratory pauses) and volume histories are imposed and controlled by the respirator (Harvard) during positive pressure ventilation (PPV). Static pressure-volume curves are obtained for the intact lungs by, starting from functional residual capacity (FRC), inflating the lung with a Hamilton Super Syringe in prescribed increments (e.g., 100 ml increments) to total lung capacity (TLC), defined as 25 cm H_2O TPP and then deflating in the same incremental manner back to FRC. Care is taken to impose the same volume history on the lungs immediately prior to doing the pressure-volume curves.

In addition to using pairs of markers to quantitate directional inter- and intralobar strains, it is possible to calculate dynamic changes in regional lung volume (i.e., ventilation). By selecting sets of 4 markers (i.e., with any given set of 4 contained within the same lobe) to define a tetrahedron, the spatial and temporal distributions of changes in regional lung volume, relative to the lung itself (i.e., in contrast to inspired radioactive gas techniques) are obtained throughout the respiratory maneuver. Furthermore, since the three-dimensional (i.e., spatial) coordinates of the tetrahedrons are known throughout the respiratory cycle, the dynamic changes in relative position of the markers, and hence the volume described by them, can be analyzed with established methods in engineering mechanics. For example, pure deformation can be separated from rigid body motion (i.e., translation and rotation) and analyzed for axial strains (i.e., ε_x, ε_y, ε_z) and shear strains (i.e., ε_{xy}, ε_{yz}, ε_{xz}) thereby providing strain tensors for different regions of the lung during a particular respiratory maneuver. Software to perform these calculations has been written and implemented on our CDC 3500 computer.

To date, 3 dogs have been studied in this plethysmograph and the results will be reported later upon completion of this phase of the study.

To aid in interpreting regional parenchymal strain data, it would be helpful to be able to visualize in three dimensions, the dynamic displacements of the parenchymal markers throughout a selected respiratory maneuver. While true three-dimensional display devices are still in the developmental stage, it is possible to obtain a pseudo 3-D or perspective display of marker displacements by looking at a 2-D image of the respective marker positions as the image is rotated about a given axis. The software required to accomplish this has been written by personnel in our laboratory and the preliminary results are shown in Figure 14. The picture depicts the anterior-posterior (i.e., ventral-dorsal) view of a dog's thorax (Z-axis vertical) with the dog's right side on the left of this picture. The white dots depict the positions of 12 markers at functional residual capacity (FRC)(i.e., at end-expiration) while the red dots represent the positions of the respective markers at total lung capacity (TLC)(i.e., maximal lung volume). The pathways that the markers took in going from FRC to TLC and back are shown by the lines connecting the white (FRC) and red (TLC) dots. Only 7 of the 15 data points for this respiratory maneuver are shown for each marker for the sake of clarity. Markers in different lung lobes are identified by the color of the lines connecting the dots (i.e., upper lobe - yellow; middle lobe - blue; and lower lobe - orange).

Figure 14 The ventral-dorsal view (Z-axis vertical) of a dog's thorax (dog's right side on left side of picture) with the marker positions identified at FRC (white dots) and at TLC (red dots) with the pathways taken by the individual markers as the lung was inflated from FRC to TLC and back to FRC indicated by the lines connecting the data points (dots). Lobar location of markers identified by color of connecting lines (i.e., upper lobe - yellow; middle lobe - blue; and lower lobe - orange).

Figure 15 represents the same data as shown in Figure 14 but rotated 90° to the right (right-lateral)(left panel) and 90° to the left (left-lateral)(right panel) to further illustrate the capabilities of this display algorithm. In fact, the image can be rotated about any axis in any desired angular increment. Furthermore, it is possible to visualize the dynamic displacements of these markers during the respiratory maneuver at any desired angle. It is hoped that these types of display options will aid in assessing regional

lung parenchymal distortions and strains as well as elucidating the role that lung fissures and lobar slippage play in influencing regional lung mechanics.

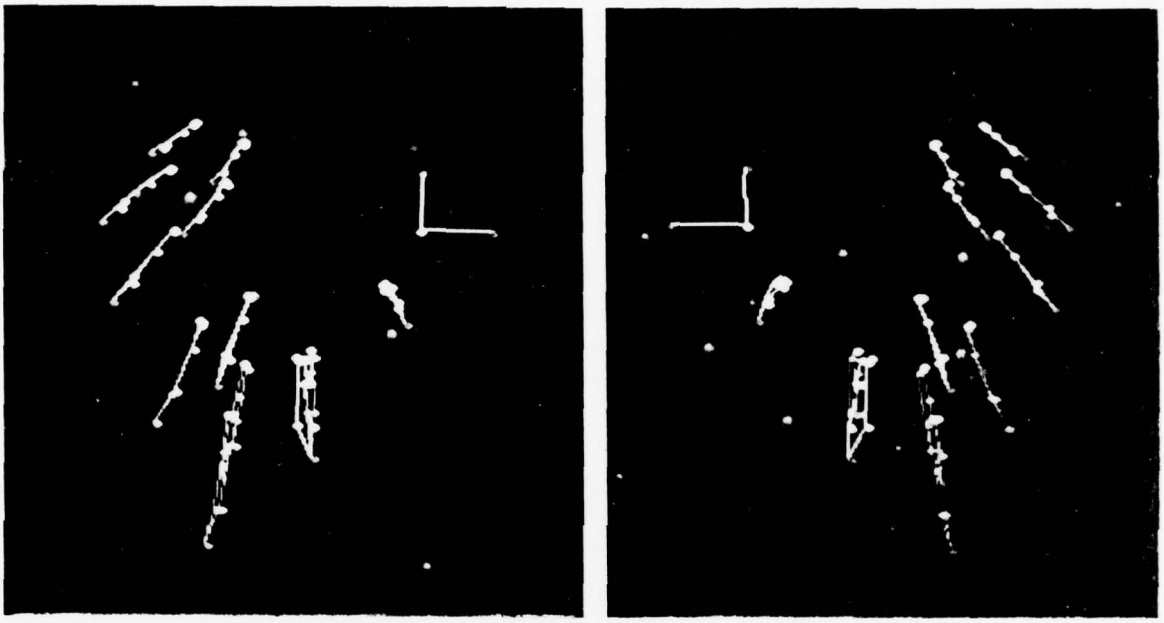

Figure 15 The right-lateral (left panel) and left-lateral (right panel) views of the marker positions in the dog's thorax in Figure 14. See Figure 14's legend for description of color codes used.

Summary and Significance (Part I)

The development in our laboratory of the parenchymal marker technique (Part I) as well as the ability to reconstruct the three-dimensional shapes and dimensions of the heart, lungs, chest wall and diaphragm, in the intact thorax (Part II) presents a unique opportunity to study dynamic regional lung mechanics and lung-chest wall-diaphragm interaction under various conditions of lung volumes and body position and thereby provides the methodology to study the effects on regional lung function of alterations in these parameters induced by changes in the gravitational-inertial force environment. The

results described in Part I represent significant new information regarding regional mechanical properties of the lung and clearly indicate the need to study the intrinsic elastic behavior of the lung and its relationship to the chest wall and diaphragm in the intact thorax with techniques possessing sufficient temporal and spatial resolution to permit quantitative determination of the dynamic changes in spatial (three-dimensional) lung parenchymal strains, regional lung volumes and lung-chest wall geometries.

Mechanical studies of the intact lung have, heretofore, not been possible. These data, which cannot be obtained by other methods, provide a quantitative measure of the mechanical properties of the lung under normal physiologic conditions (i.e., an intact thorax and normal intrathoracic pressures) at 1G and will preface similar planned studies under conditions of increased or decreased gravitational-inertial force environments encountered in aerospace flight.

Because of the very large differences in specific gravity of the air in the alveoli, and the lung parenchyma and its mobile blood content plus the anatomically fragile nature of the lungs, the respiratory system is the most susceptible of all bodily organs to malfunction and actual structural damage during exposure to changes in the direction and magnitude of the gravitational-inertial force environment.

Consequently, increased knowledge concerning the mechanical characteristics and dynamic three-dimensional geometry of the lung is a basic requirement for understanding the factors which determine man's reactions and tolerance to short and long term changes in the force environment such as encountered in conventional aircraft and in manned space flight.

PART II: Dynamic Spatial Reconstruction Tomography for Quantitative Studies of Structure and Function of the Heart, Lungs, and Circulation

A. Overview and Current Status of X-Ray Techniques for Reconstruction and Display of Moving Organ Systems

Two major activities in our laboratory during the past four years have opened the door to development of procedures for true, dynamic three-dimensional imaging of the heart, lungs, and circulation; namely, 1) development of the capability for high quality recording and rapid computer digitization of multiplanar x-ray video projection images (8,12) and comprehensive display of quantitative image and functional data derived therefrom, and 2) computer implementation of a fan beam cross-sectional reconstruction algorithm, called ART III (13,14), which is similar in concept to that employed in the first EMI brain scanner but which works satisfactorily with a relatively low number of two-dimensional x-ray fan beam projections recorded with our video fluoroscopic system.

The capability provided by the video image digitizing system for obtaining high spatial resolution (up to 2,000 samples, each 0.1 mm apart, on each of 250 lines per video field, each line 1 mm apart) and high temporal resolution (60 video fields per second) measurements of the changes in x-ray densities and the distribution of these densities throughout organs such as the heart and lungs is required for determination and display of the true dynamic cross-sectional geometry of these organs.

In addition to the algebraic reconstruction technique, ART III (13), we have implemented on our CDC 3500 computer a convolution reconstruction algorithm (15) which also operates on x-ray fan beam multiplanar projection data. If enough views can be collected (60 or more), the convolution algorithm produces more accurate cross-sectional images in less time than are obtained with the algebraic technique. For 64 x 64 reconstructions from 60 views, approximately 3 minutes are required if ART III is used, whereas about 1 minute is required if the fan beam convolution algorithm is used.

Figure 16 diagramatically illustrates the system developed in our laboratory for generation and collection of two-dimensional multiplanar x-ray projection images for dynamic spatial reconstructions of the thorax using a computer-controlled single-source single-detector x-ray fluoroscopic system. The x-ray imaging chain, shown at the bottom of the figure, is a new high performance video-fluoroscopic system, unique in its design and construction, which is called the SSDSR for single source dynamic spatial reconstructor (see Appendix I).

This assembly has the advantage that the entire thorax of medium sized dogs can be imaged on the large 12" x 12" flat screen ($GdSO_2$) with minimal geometric distortion. This cannot be done with the conventional 9" diameter, curved screen electrostatic image-intensifier tubes. In addition, the two-stage magnetically-focused image-intensifier and image-isocon video camera have far superior dynamic range, spatial resolution, and lag characteristics by comparison with conventional fluoroscopic systems (16, Appendix I).

DIAGRAM OF COMPUTER-CONTROLLED SINGLE-SOURCE SINGLE-DETECTOR X-RAY VIDEO SYSTEM FOR COLLECTION OF MULTIPLANAR ROENTGEN VIDEO PROJECTIONS FOR DYNAMIC SPATIAL RECONSTRUCTIONS OF THE INTACT THORAX AND ITS CONTENTS

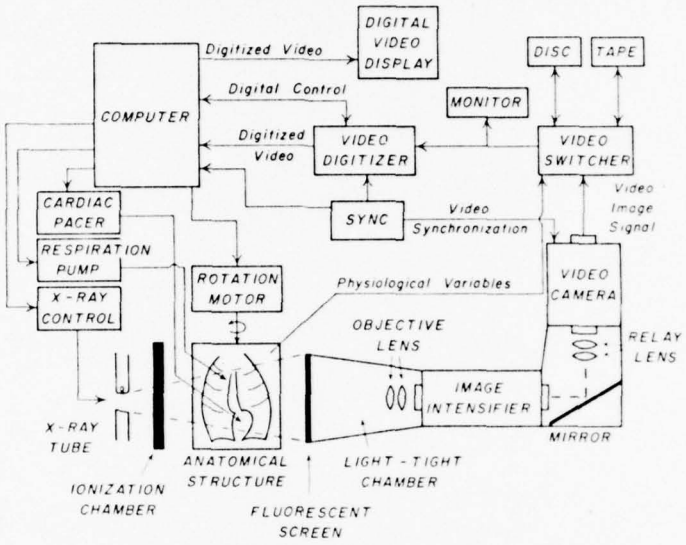

Figure 16 Diagram of computer-controlled single-source dynamic spatial reconstruction system (SSDSR).

The object to be reconstructed is positioned in the x-ray field of the SSDSR and rotated under computer-control about an axis perpendicular to the central plane of x-ray beams. The fluoroscopic image at each successive angle of view is scanned by the video camera, producing an electronic video signal representation of the image, which is made up of up to 250 scan lines for maximum (60/sec) temporal resolution reconstructions of the beating heart or up to 500 horizontal scan lines for reconstructions of slower moving structures (17).

Each line in the video image represents the projections of an approximately 0.5 mm thick section of the object scanned. Measurements of the transmitted x-ray intensities on each video line are made by the video digitizer (12) and are repeated on the same lines for each successive view of the object as it is rotated in

equi-angular increments through a total arc of 180° to 360°. The video digitizer can digitize up to 1000 points on a single line in real time, or the entire video image in about 10 seconds. These x-ray transmission measurements provide the data required for determination of up to 500 parallel adjacent cross sections of the object, or, in other words, its complete three-dimensional reconstruction.

Reconstruction of a moving object, such as a beating heart within the thorax of a live animal, using a single x-ray source imaging system, requires maintenance of exact temporal relationships between physiological events and x-ray projection image recording. This is accomplished by slaving all components of the system, including the computer, to the master oscillator, labeled SYNC in Figure 16, which controls the video sweep circuits of the video camera. The rate and phase of the cardiac and respiratory cycles are kept constant and synchronized with the rotation, x-ray pulses, video recording and digitizing process by computer-controlled ventilation of the lungs and pacing of the atria and ventricles, all in exact phasic relationships with each other and with the 60-per-second oscillator pulses. The ECG and other hemodynamic variables are simultaneously recorded with the video images on a video tape or video disc (8) so that sets of images recorded at the same phase of successive respiratory and cardiac cycles at each incremental angle of view can be selected for each 60-per-second point in time throughout the respiratory and cardiac cycles to obtain dynamic spatial reconstructions of the full anatomic extent of the thorax and its contents.

Figure 17 schematically illustrates how a single transverse cross section of an object like the heart may be determined using an algebraic reconstruction technique.

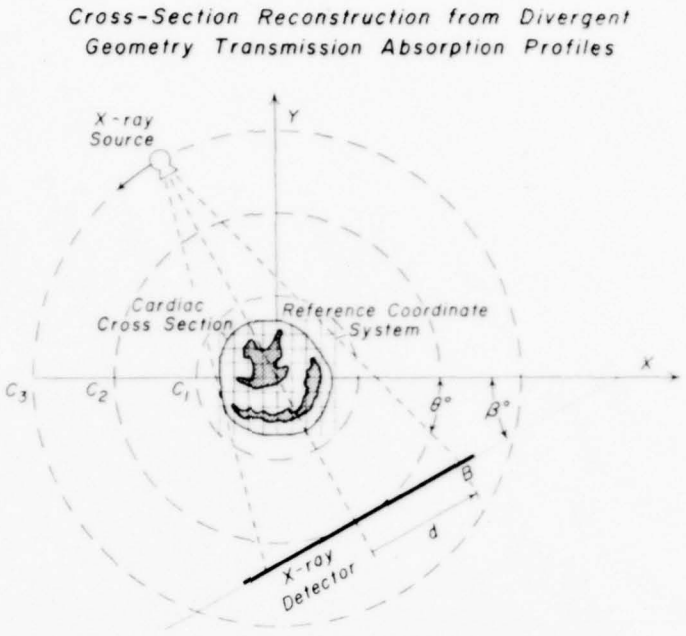

Figure 17 Diagram of geometric considerations for transaxial x-ray reconstruction of a cross section of the heart.

The transaxial plane traversed by the x-ray beam which contains the desired cross section of the object to be reconstructed is mathematically divided into a number of small squares (typically from 64 x 64 up to 128 x 128) and the intensity of the x-ray beam transmitted through that plane is measured at several points (typically from 200 to 500) along the detector for each rotational position of the x-ray source and detector with respect to the object. The geometric considerations are the same if the source and detector are rotated about the object or if the object is rotated with respect to a fixed source and detector. The transmitted x-ray beam measurements from the detector are related to measurements of the incident x-ray beam (obtained by removing the object from the system)

for all angles of view by a system of linear equations in which the unknowns are the x-ray beam attenuation coefficients in each small square of the grid. The algebraic solution of this system of equations provides an array of numbers which are proportional to these x-ray attenuation coefficients and which can be displayed as a matrix of picture elements with individual brightness levels proportional to the attenuation coefficients in each small square. Such a display results in an image of the cross-sectional structure of the object scanned. The detector in this figure can be considered to be 1 video line of the up to 500 video lines in our x-ray fluoroscopic system, each of which can be used to reconstruct cross sections over the entire anatomic extent of the heart or thorax.

The left-hand panel in Figure 18 is a photograph of the x-ray video image of the thorax of an intact dog recorded with the SSDSR system during rotation of the dog through 360°. The white area on either side of the chest in each image represents the unattenuated x-ray beam impinging on the fluorescent screen and demonstrates the superior dynamic range of this system, by comparison to conventional fluoroscopic equipment, inasmuch as the spine can be seen through the heart shadow, and other intrathoracic structures, including the radiopaque 2 mm diameter catheters, simultaneously with segments of the image produced by the unattenuated x-ray beam. No x-ray contrast material has been injected into the dog to produce this image.

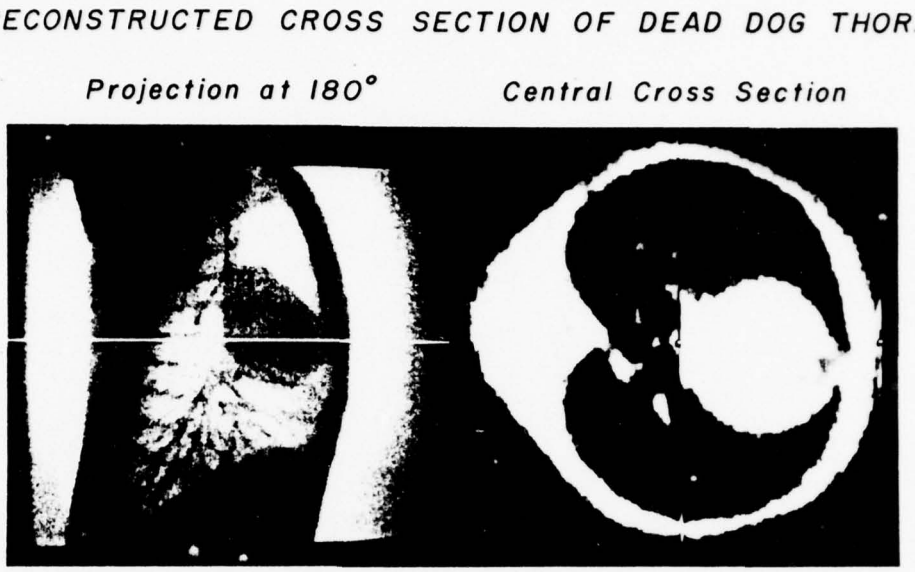

Figure 18 X-ray video projection image of intact dog thorax recorded with SSDSR (left) and reconstructed cross section of the thorax (right) at level indicated by brightened line.

The vertical column of bars at the left of each image are the amplitude-modulated analog signals of up to 16 hemodynamic variables, including ECG, pressures, etc., which are simultaneously recorded with the video images (8). The brightened line indicates the level of the reconstructed cross section of the thorax shown in the right panel.

This reconstruction, produced by a fan-beam convolution algorithm, contains 117 x 117 picture elements and was determined from 120 views recorded over a range of 360°. Note the spinal vertebra and spinal cord, ribs, pleural surfaces of the lungs, the esophagus, bifurcated trachea, epicardial surfaces of the heart, and the two catheters (2-mm diameter) in the heart. Some trapped air introduced via the intracardiac catheters can be seen in the chambers of the heart of this dead dog. The spatial and contrast resolution achieved in this reconstruction is very encouraging, considering that conventional (4 ma) fluoroscopic x-ray levels and video recording techniques were used.

The top panel in Figure 19 depicts 12 brightened 0.5 mm thick video lines, each 16-mm apart, covering the anatomic extent of the thorax of an intact dog. These levels were selected from one 360°, circumferential scan for reconstruction of 12 cross sections of the dog's chest. The video lines just above and below each brightened level were also digitized and averaged with the selected lines. Since the midpoints of adjacent lines are spaced at 1.0 mm intervals, averaging of 3 lines results in a cross section which encompasses an approximately 3 mm thick section of the scanned object.

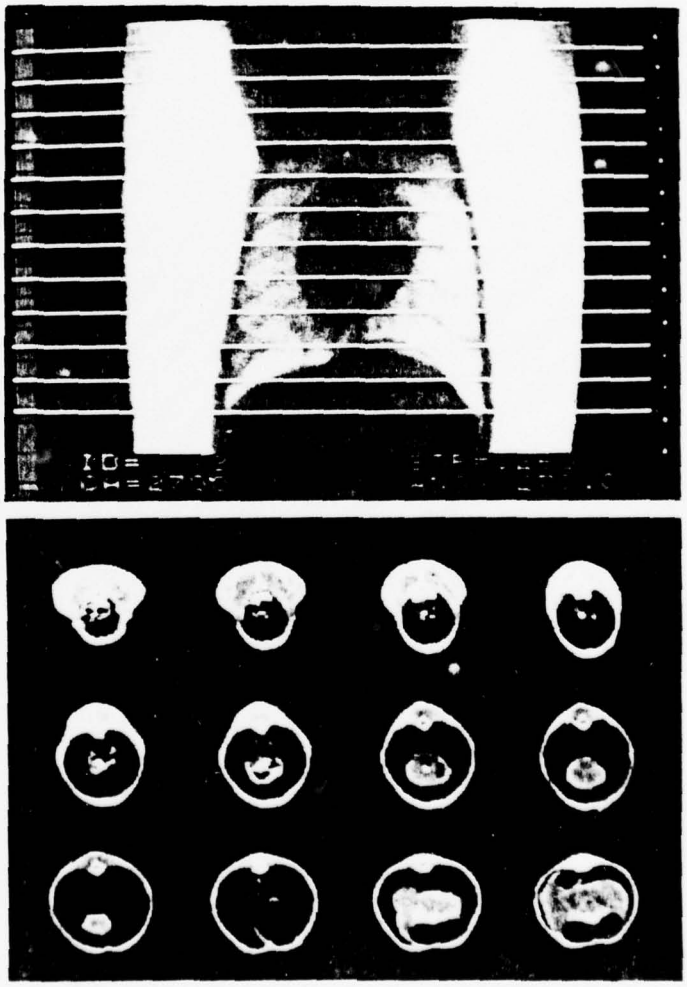

Figure 19 X-ray video projection image of dog thorax with superimposed lines (top) at 12 anatomic levels selected for cross-section reconstruction, and 12 separate 3-mm thick transverse sections through thorax (bottom) reconstructed at selected levels, extending from the apex to the base of the lungs.

The bottom panel in Figure 19 shows these 12 reconstructed cross sections of the thorax from the apex of the lungs, at the upper left of the panel, extending cephalocaudally to the base of the lungs, at the lower right of the panel, in left-to-right, top-to-bottom order. Each cross section contains 64 x 64 picture elements and was reconstructed in approximately 1 minute from 60 equally spaced views over 360° by a fan-beam convolution algorithm. The spinal vertebra, ribs as they course through the plane of the cross section, the esophagus and bifurcated airway, the epicardial surface of the heart, the pleural surfaces of the lungs, and the diaphragm can all be visualized at the appropriate levels. Air in the transverse segment of the large intestine can be seen in the lower row of cross sections. No x-ray contrast material was injected into the dog to obtain these reconstructions.

A very useful advantage of full spatial anatomic reconstructions of the thorax such as those shown in Figure 19 is that multiple parallel sections oriented at <u>any desired angle</u> in relation to the x, y and z axes of the thorax can be computed from the reconstructed <u>transverse</u> images, and displayed for viewing of the thorax from any desired aspect.

The top panel in Figure 20 is a photograph of the A-P x-ray video projection image of the dog's thorax, which contains all of the structures of the thorax superimposed upon the recording plane. The bottom panel in Figure 20 is a computer-generated display of 12 separate, parallel 3-mm thick <u>coronal</u> sections through the thorax, extending from the sternum at the upper left to the backbone at the lower right. These 3 mm thick coronal sections of 64 x 64 picture elements each were computed from 64 reconstructed transverse sections of the chest, of which 12 are shown in Figure 19. Note the ribs in the chest wall, the catheters in the heart (first and second images in row 2), the trachea and esophagus (third and fourth images in row 2, respectively) and the detail of the vertebral column (in row 3).

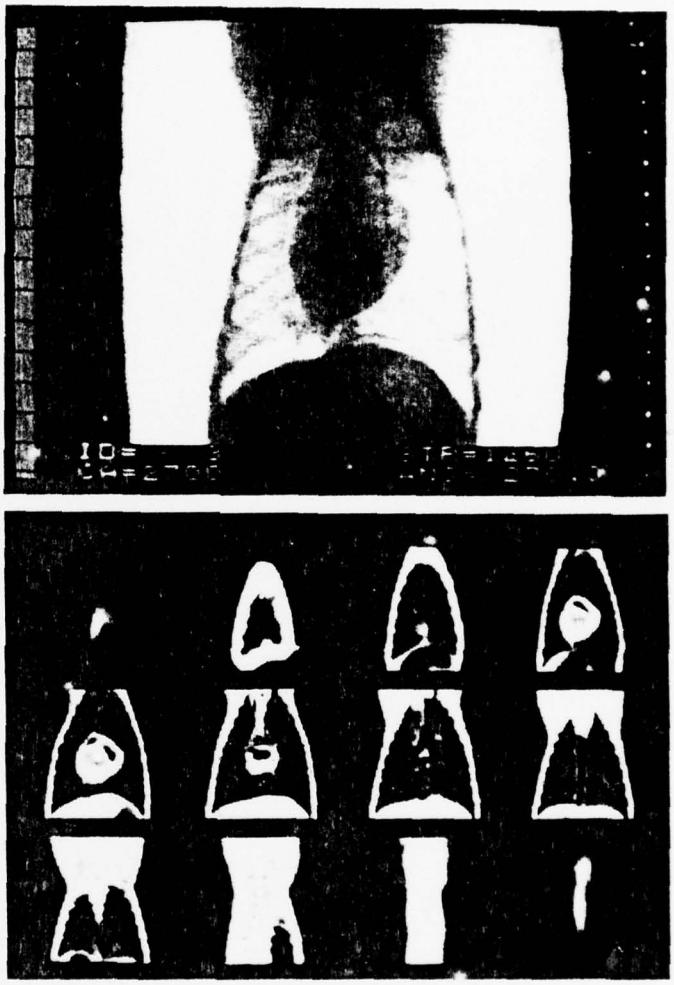

Figure 20 X-ray video projection image of dog thorax (top) recorded in anterior-posterior position, and 12 separate 3-mm thick coronal sections of the thorax (bottom) extending from the sternum to the backbone, computed from the same scan data and spatial array x-ray attenuation values encompassing the full thorax, used for the reconstructed sections shown in Figure 19.

Figure 21 is a similar display with a lateral x-ray video projection image of the dog's thorax shown in the top panel and 12 separate, parallel 3-mm thick sagittal sections shown in the bottom panel. These sections extend from the left side of the thorax (at the upper left) to the right side of the thorax (at the bottom right) and were computed from the same set of 64 reconstructed parallel transverse cross sections as were used to compute the coronal sections shown in Figure 19. The intrathoracic structures are again clearly visible. Note particularly the shapes of the heart and lungs, the catheter traversing the cephalo-caudad extent of the superior vena cava (2nd image) and in the right atrium (3rd and 4th images, row 2), and the detail of the spinal vertebrae, also in the second row of images.

To further illustrate the advantages of full spatial (3-D) reconstructions of the thorax, Figure 22 shows, in the top panel, 12 sections through the cephalo-caudad mid-line (Z-axis) of the thorax, with each successive section from left-to-right and top-to-bottom representing a slice directly through this central vertical axis but rotated by 24° with respect to the previous section. The 12 images shown in the bottom panel of Figure 22 are parallel oblique sections computed at an angle of 45° to each of the x, y, and z axes of the thorax. This slice orientation is nearly parallel to the longitudinal base-to-apex axis of the heart. The multioriented "thin" sections in figures 19-22, all of which were computed from one synchronous cylindrical scan of the thorax, demonstrate the capability for detailed quantitative analysis of simultaneous anatomical structure and functional relationships of intrathoracic or other organ systems of the body.

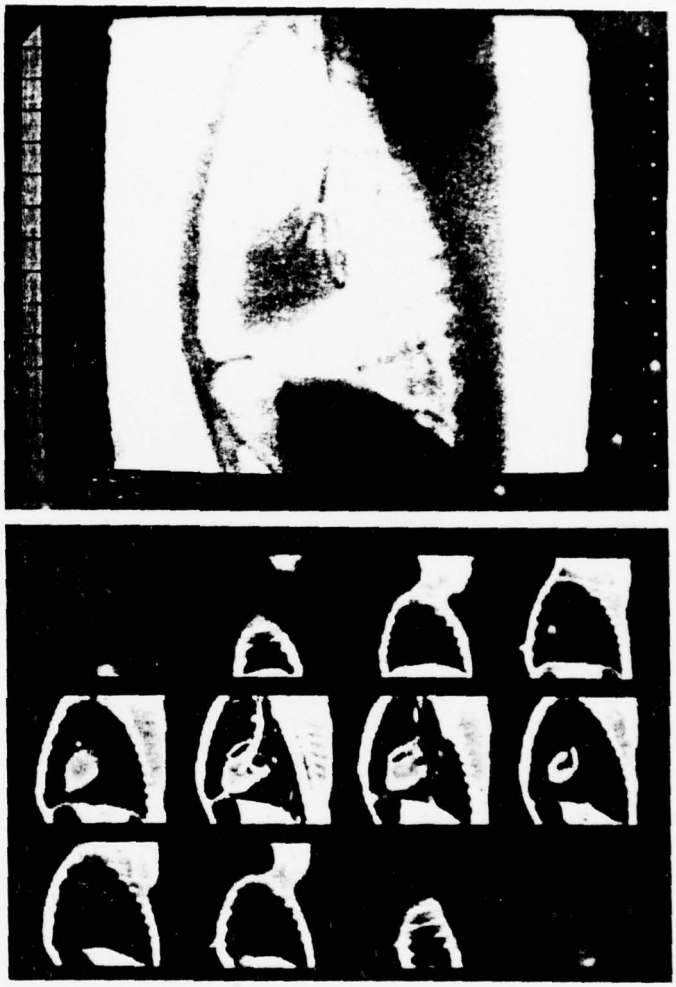

Figure 21 X-ray video projection image of dog thorax (top) recorded in left-lateral position, and 12 separate 3-mm thick sagittal sections of the thorax (bottom) extending from the left chest wall to the right chest wall, computed from the same scan data and spatial array of x-ray attenuation values determined for Figure 19.

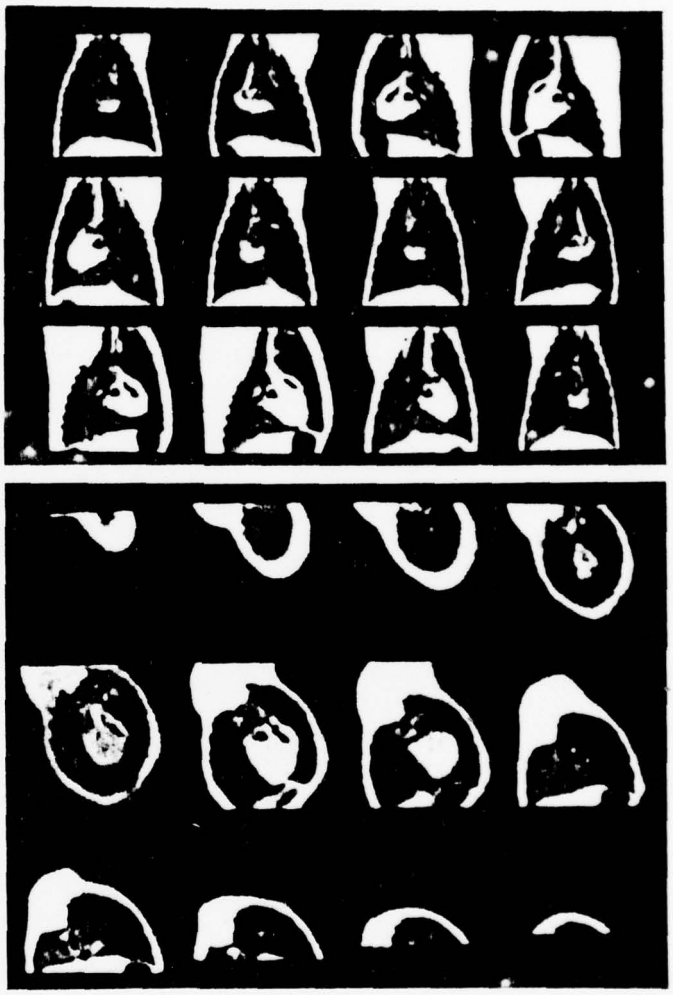

Figure 22 Twelve longitudinal thoracic sections (top) computed at 24° angular increments through cephalo-caudal midline (z-axis) of dog thorax, and 12 parallel oblique thoracic sections (bottom) computed at 45° angle to x, y, z axes of thorax from the same scan data and resulting x-ray attenuation values as used for Figure 19.

However, in order to accurately study dynamic structural-functional relationships of moving organ systems, it is necessary to obtain high temporal resolution (i.e., 60 to 100 times per second) three-dimensional reconstructions of these structures. This can be accomplished by the SSDSR in dogs during imposed conditions of "physiological stationarity" produced by precise computer control of the rate and magnitude of the respiratory and cardiac cycles in exact interphasic temporal relationships with the multiplanar x-ray video image scanning and recording procedures.

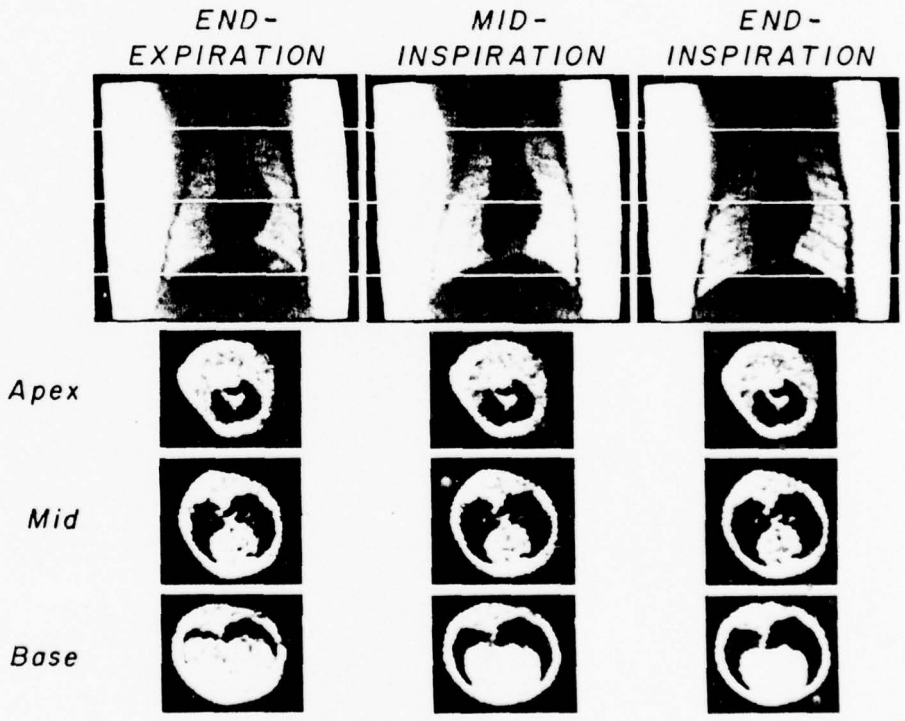

Figure 23 X-ray video projection images of living dog's thorax (top row) recorded in anterior-posterior position during 3 phases of respiratory cycle, and reconstructed cross sections of thorax (bottom three rows) for these 3 phases of respiratory cycle at 3 different anatomic levels of thorax, indicated by brightened horizontal lines.

Figure 23 illustrates a sequence of thoracic cross-sectional reconstructions of a living dog's chest, with no x-ray contrast material injected, obtained from temporally correlating sets of digitized multiplanar x-ray images of the thorax recorded during computer-controlled ventilation, cardiac pacing, and rotation of the dog in angular increments of 6° on successive respiratory cycles for a total of 31 cycles (i.e., 31 views over 180°). The top row of projection images, from left-to-right, were recorded at the end-expiratory, mid-inspiratory, and end-inspiratory phases of the respiratory cycle, respectively. The brightened horizontal lines on each image depict three levels near the apex, center and base of the thorax selected for reconstruction at these three phases of the respiratory cycle. Each row of cross sections (reconstructed using ART III, due to the limited number of views) represents the three selected anatomic levels of the chest. The top, center, and bottom rows correspond respectively to the apical, mid, and basal levels of the thorax. Each column of cross sections represents the three different phases of the respiratory cycle. The left, center, and right columns corresponding respectively to the end-expiratory, mid-inspiratory, and end-inspiratory phases of the respiratory cycle. Hence, this montage of images illustrates both dynamic (in the horizontal direction) and spatial (in the vertical direction) reconstructions made from a single circumferential scanning procedure.

The top two panels in Figure 24 are x-ray video projection recordings of a beating heart in an intact living dog at end-diastole (left) and end-systole (right). The brightened horizontal line depicts one of approximately 80 to 100 levels of the heart, extending from base-to-apex, which could be selected for cross-sectional reconstruction of the heart during the cardiac cycle. During rotation of the dog in 6° increments on every other beat through a total

range of 180°, yielding 31 views in a total scan time of approximately 25 seconds (heart rate was 150 beats/minute), respiration was suspended and x-ray contrast material was infused continuously into the left ventricular chamber to achieve continuous opacification of the chamber during the rotational scan period.

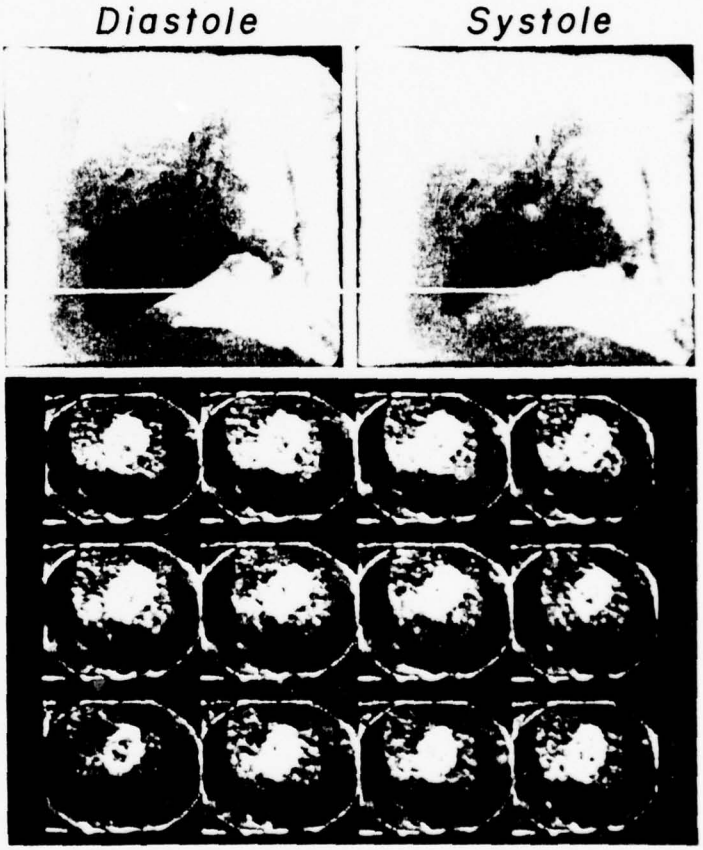

Figure 24 X-ray video projection images of beating heart in intact dog (top) recorded at end-diastole and end-systole during infusion of x-ray contrast media into left ventricle, and cross section of intact beating heart (bottom) reconstructed at level of brightened line for 12 points in time throughout the cardiac cycle.

The lower three rows of panels in Figure 24 show a single cross-sectional level near the mid-plane between the base and apex of the heart which was reconstructed (using ART III) at 12 successive points throughout the cardiac cycle, with each successive point in time being 33 msec apart.

The left ventricular chamber and epicardial surfaces of the heart can be seen in each successive image in the first two rows of cross sections during the isovolumic and contractile phases of the systolic period, followed by the subsequent diastolic filling period shown in the bottom row. The upper left hand cross section corresponds to end-diastole, and is coincident with the computer pacing pulse (or "R" wave) which initiates the contraction.

These cross sections demonstrate the heretofore unobtainable capability for obtaining the dynamic cross-sectional shape and dimensions of both the epi- and endocardial surfaces of the intact working heart in living animals over the entire anatomic and temporal extents of the myocardial walls and cardiac cycle, respectively.

In order to study left ventricular dynamics in greater detail, ideal roentgenographic conditions, using an isolated, working canine left ventricle, were arranged. The top row of panels in Figure 25 are x-ray video images of an isolated left ventricle shown at end-diastole and at end-systole before and after ligating the anterior branch of the circumflex coronary artery. The two brightened lines near the mid-level and apex of the isolated ventricle depict the anatomic levels selected for reconstruction of the cross sections of the ventricle shown in the bottom two rows of panels. The coronary circulation, supplied by arterial blood from a donor dog, was kept completely separate from an artificial systemic circulation, which contained 10% Renovist in solution

with isotonic Ringer's dextran to provide continuous, beat-to-beat, roentgen opacification of the chamber. During computer-controlled rotation of the isolated ventricle, both before and after the circumflex coronary artery was tied off, the heart rate was controlled by electrical pacing pulses which were synchronized with the video scan rate to ensure a fixed temporal relationship between the 60-per-second x-ray images recorded at each angle of view and the mechanical phases of each successive cardiac cycle. The ventricle was rotated during alternate cardiac cycles so that one complete cardiac cycle was recorded at each angle of view.

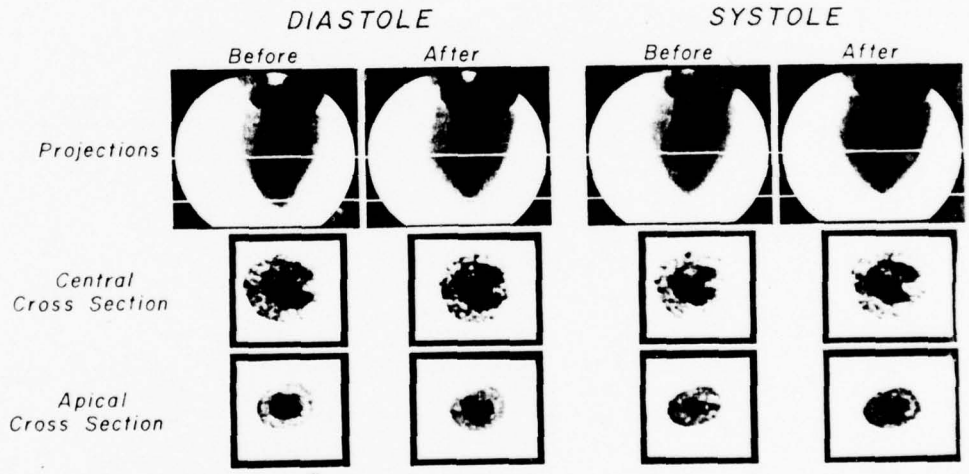

Figure 25 X-ray video projection images of beating isolated canine left ventricle (top row) recorded during diastole and systole before and after ligation of circumflex coronary artery, and reconstructed cross sections of ventricle (bottom two rows) at 2 levels indicated by brightened lines, determined for diastole and systole before and after ligation of the circumflex coronary artery.

Although not discernible in the projection images, the reconstructed cross-sectional images in the bottom two rows of Figure 25 indicate the functional effect of the diminished supply of blood to the anterior wall of the left ventricular myocardium. In the first row of cross sections, which show the mid-level of the left ventricle at end-diastole before and after ligation (left two panels, respectively) and at end-systole before and after ligation (right two panels, respectively), the anterior and posterior papillary muscles can be clearly seen. The cross-sectional area of the chamber at this mid-level is noticeably greater in the images reconstructed after the artery was ligated, indicating the weakened contractile capability of the ventricular myocardium. At the apical level (bottom row of cross sections), the end-systolic cross-sectional area is significantly larger in the image reconstructed after ligation of the coronary artery. By determination of the borders of the endocardial and epicardial surfaces in these cross sections (by tracing with a light pen or using automatic edge detection techniques (21)) accurate quantitative analysis of regional left ventricular structure and function (e.g., dynamic chamber dimensions, wall thickness, rate of wall thickening, contractile patterns, etc.) can be carried out and studied under a variety of known and controlled conditions.

Figure 26 is a computer-generated gray level plot of two cross sections of an isolated beating left ventricle reconstructed near the base (left) and apex (right) of the ventricle during the same instant in the cardiac cycle. The myocardium is depicted by points with different gray levels which are proportional to the degree of stress at each point location in a direction perpendicular to the plane of the reconstructed cross section. These values are determined by mathematically dividing the cross-sectional image of the myocardium into a linked set of several hundred triangular elements and, by using finite element analysis techniques (19), computing the stresses at each node of each triangle on the basis of the cross-sectional shape of the myocardium and the simultaneously measured

transmural cardiac pressures. This type of display in which measured or calculated physiological variables are superposed upon the reconstructed cross-sectional anatomy permits simultaneous analysis of structure and function of the object being studied.

Figure 26 Computer-generated stress plots for two cross sections of left ventricular myocardium reconstructed at basal (left) and apical (right) levels at same point in diastolic phase of cardiac cycle.

Display of the three-dimensional image information obtained by computerized tomographic techniques is an important factor in establishing the usefulness of these capabilities in basic research and clinical practice. Time delay video and cine recordings of the temporal and spatial sequences of the computer-generated cross-sectional reconstructions illustrated in these figures have been made. These sequences of cross sections reconstructed over the full anatomical extent of the beating heart and breathing

lungs throughout successive cardiac and respiratory cycles, respectively, in isolated preparations and in intact dogs can be viewed in variable time base modes ranging from stop-action to real-time. Such dynamic displays provide the capability for studying the spatial relationships and instant-to-instant changes in geometry of these organs and permits evaluation of their regional and integrated overall function in the intact thorax (20).

Examples of how three-dimensional images can be displayed to permit analysis of the spatial relationships and regional detail of image structures is illustrated in Figures 27 and 28.

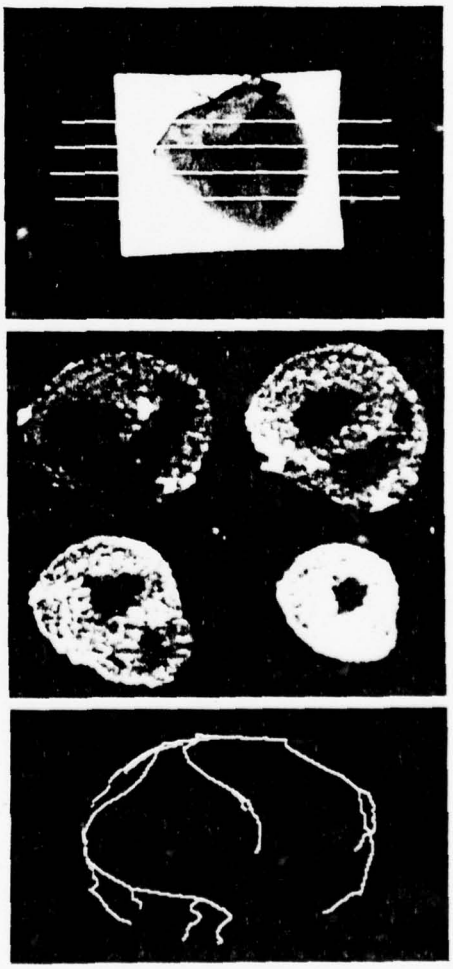

Figure 27 X-ray video projection image of isolated intact canine heart (top) with coronary arteries filled with x-ray contrast material, and 4 cross sections

of heart (center) reconstructed at anatomic levels indicated by brightened lines, and perspective 3-D display of coronary artery tree (bottom) computed from x,y,z coordinate positions of coronary arteries in 48 reconstructed cross sections of heart.

The top panel in Figure 27 is an x-ray video image of an isolated intact canine heart whose chambers and coronary arteries were filled with cotton and barium paste, respectively, prior to rotation and digitization of four video lines selected for cross-sectional reconstruction.

The center panel shows the reconstructed cross sections at the four levels indicated by the brightened horizontal lines in the top panel. The characteristic cross-sectional shapes of the epi- and endocardial surfaces of both the left and right ventricles at each level are accurately reconstructed. In addition, the cross sections of the coronary arteries as they traverse the myocardial walls can be seen as bright spots (more x-ray dense) at each cross-sectional level. These arteries are approximately 2-mm in diameter near the base of the heart (upper-left cross section) and 0.5 mm in diameter near the apex of the heart (lower-right cross section).

The bottom panel in Figure 27 is a three-dimensional perspective line display of the coronary tree of the heart determined from the coordinate positions of the coronary arteries, which were entered into the computer using an operator-interactive display and light pen assembly, in each of 48 parallel cross sections of the heart reconstructed from its base to apex. By performing rotational matrix operations on these sets of x, y, z coordinates, line representations of the coronary tree can be viewed from any orientation in stop-action or during continuous rotation to facilitate studies of the geometric relationships of the coronary artery system.

Similar three-dimensional displays of the complete coronary vessels, obtained by entering into the computer complete sets of reconstructed sections encompassing the full extent of the large coronary arteries permits computation of regional cross-sectional lumenal areas of these arteries for more accurate detection and quantitation of regional stenosis or occlusions.

Application of three-dimensional boundary surface detection and three-dimensional computer graphics techniques to three-dimensional reconstruction data (21) provides the capability of three-dimensional displays of solid objects.

The upper left panel in Figure 28 is a computer-generated three-dimensional surface display of an isolated canine heart which was determined by automatic three-dimensional boundary detection of 30 reconstructed cross-sectional levels of the heart. The upper right panel in Figure 28 is a similar display of the same heart rotated 90° and tilted forward 15°. The bottom panel in Figure 28 is a three-dimensional gray-level surface display of the same heart but mathematically opened into halves to permit viewing of the structural detail of the endocardial surfaces.

The capability provided by the video image digitizing system (12) for obtaining high spatial (up to 2,000 samples on each of 250 lines per video field) and high temporal (60 video fields per second) resolution measurements for cross-sectional reconstruction of moving organs also permits the study of the appearance, mean transit and clearance of x-ray contrast substances through, for example, the myocardium with a degree of anatomical and temporal precision not possible by current radioisotope techniques.

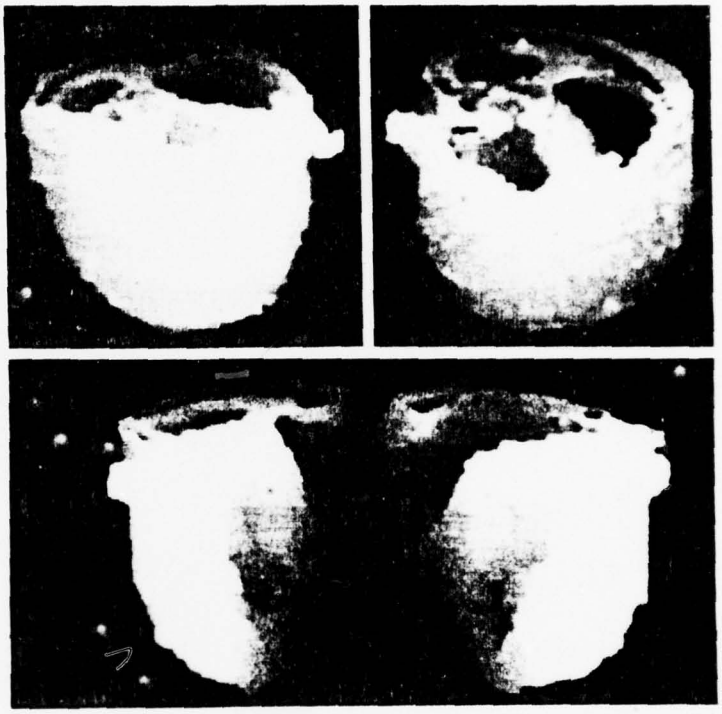

Figure 28 Computer-generated three-dimensional gray-level displays of isolated intact dog heart determined from 30 reconstructed cross-sectional images extending from base to apex of heart.

This capability is indicated in Figure 29 which illustrates the quantitative determination by dynamic background subtraction of the spatial distribution of the coronary circulation within the myocardium of a patient undergoing selective coronary arteriography. The computer-generated difference images (4 right-hand panels) of contrast distribution at the same specific phase of four successive heart beats were obtained by subtraction, sample for sample, of the digitized arrays of the actual video images (4 left-hand panels), recorded during and following the injection of contrast material, from the digitized arrays of the video images

recorded just prior to the injection. Simultaneous ECG recording on the videotape allows precise temporal and phasic registration between the pre-injection video images and the post-injection video images which are subtracted to produce difference pictures at each point in the cardiac cycle throughout successive post-injection cycles.

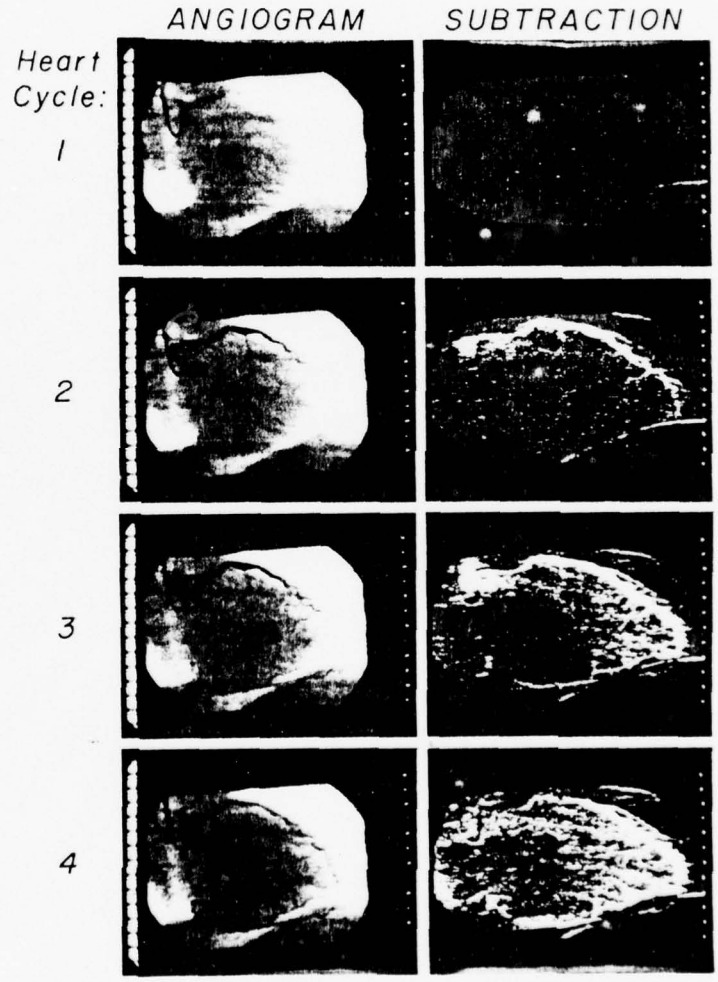

Figure 29 X-ray video images of human heart (left column) recorded at same phase of diastole in 4 successive cardiac cycles during selective coronary angiography, and computer-generated difference images of the heart (right column) determined by dynamic background subtraction for this same phase of these 4 cardiac cycles before, during, and following injection of x-ray contrast material into the left anterior descending coronary artery.

The display of the difference images greatly enhances the ability to see the myocardial perfusion patterns of the microvascular anatomy and demonstrates the potential capability for quantitative evaluation of myocardial ischemia and infarction.

By combining dynamic three-dimensional reconstruction techniques with dynamic subtraction techniques, the instant-to-instant regional changes in shape and dimensions and transmural perfusion of the myocardium (and other organ systems) can be accurately and completely studied.

B. Physiologic Considerations in the Trade-Off Between Temporal and Spatial Resolution for Reconstruction of the Dynamic Cardiac, Pulmonary and Circulatory Anatomy and Simultaneous Functions

An ideal computerized transaxial scanner should be capable of producing reconstructions of multiple synchronous parallel sections in any desired orientation and encompassing the complete anatomic extent of the structure of interest. These juxtaposed cross sections should have sufficient three-dimensional spatial and temporal resolution for visualization and quantitative study of anatomic static and dynamic structural relationships to biologic functions of all macroscopic anatomic structures of interest including the heart, lungs, vascular anatomy and circulatory functional dynamics in all regions of the body.

Since reconstruction images are projection images, they do present ambiguous information due to superposition of structures or non-uniformities in the axial direction, just as in conventional projection images, in proportion to the thickness of the imaged structure.

The spatial and density resolution and precision of current commercial scanners is impressive (22), but only for stationary objects with concomitant uniform structure in the axial direction and uniform cross-sectional dimensions throughout and parallel to the axial extent of the cross section. Since biologic structures usually exhibit three-dimensional structural and dimensional variability the precision of their cross-sectional reconstruction depends on the degree of this variability. The significance of this limitation depends upon the nature of the study, i.e., the geometry of the organ relative to the scan thickness, motion of the organ, and the type of information which it is hoped to derive from the cross-sectional image.

The present study was undertaken to study the possible magnitude of the effects of these factors on the ability to measure the true shape and dimensions of biologic structures. The cylindrical scanning, single source, dynamic spatial reconstruction system (SSDSR) (see Appendix I) was used to provide the data for most of the results reported here. Constrained ART was used to reconstruct the cross-sectional images from profile scans obtained at thirty-five angles of view equally spaced around a circumferential scanning range of 180°.

Effect of Thickness of the Section Scanned

Figure 30 shows a stop-action display from a video disc of a monoplane video roentgenogram of a urethane cast of the myocardium of the left ventricle of a dog with the chamber filled with a dilute Renovist solution (25 mgm iodine/ml solution) in saline. The horizontal plane containing the central fan beam of the roentgen fluoroscopic system is designated by the brightened horizontal line midway between the base and apex of the cast. The urethane cast, which has the complex shape and dimensions and a roentgen

density similar to the left ventricular myocardium, has the advantage that it can be physically sliced into multiple parallel cross sections at the same levels (beads glued to surface of cast identify these levels) selected for cross section reconstructions. The slices of the cast then serve as true standards against which the shape and dimensions of the cast determined from reconstructed cross sections can be compared.

(Chamber Filled with Renovist Solution, 25 mg I/ml)

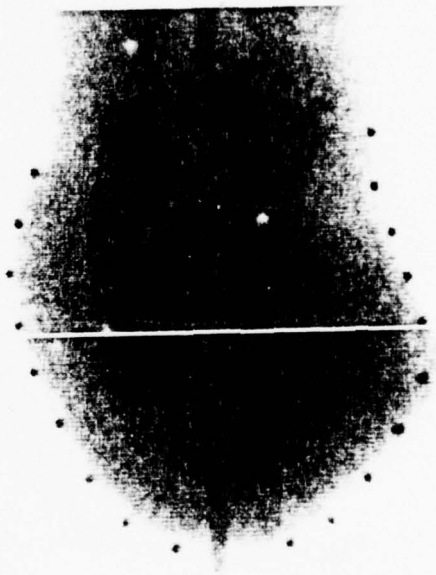

Figure 30 A single videoroentgenographic view of urethane cast of canine left ventricle with chamber filled with dilute solution (25 mgm iodine/ml) of Renovist in saline. The cast was transfixed with a 3 mm diameter aluminum rod for mechanical circumferential multiplanar "cylindrical" scanning for reconstruction of multiple juxtaposed cross sections. The dark circular objects are 1 mm lead beads, attached to the "epicardial" surface for fiducial points.

Figure 31 illustrates the accuracy of reconstructed cross sections of this urethane cast of the left ventricle, as determined by tracing with an operator-interactive graph pen the reconstructed cross-sectional outlines of the epi- and endocardial surfaces of the left ventricular cast at 21 levels from base-to-apex, and comparing the cross-sectional areas computed from these outlines with those computed from planimetry measurements of the epi- and endocardial surfaces of the corresponding actual cross sections of the cast. The mean difference between outlines (shapes) of the actual and reconstructed cross sections for all levels was 0.6 mm $\pm$ .39 mm for the epicardial surfaces and 0.83 mm $\pm$ 0.59 mm for the endocardial surfaces. An actual slice of the cast taken from its central portion and a reconstructed slice determined near the same level (indicated by brightened line in Figure 30) are shown at the top of Figure 31. Correlation of the areas determined from the actual and reconstructed cross sections were very good as shown in the regression analysis plot at the bottom of Figure 31. Accuracy of chamber volume and myocardial mass were determined to be within 5% of the true values, the major limitation responsible for the uncertainty being the 1 mm^2 size of the individual pixels in the array which constitutes the image (23). Similar accuracy of reconstruction has been shown using other test objects with both simple and complex geometric configurations (24).

The effect of the thickness of the scanning plane is illustrated in Figure 32 which shows comparisons of 0.3 mm thick slices (1 video scan line) and 10.2 mm thick slices (17 video scan lines averaged together) at three levels; 10 mm above the central plane (top pair), at the central plane (center pair), and 20 mm below the central plane (bottom pair) of the ventricular cast. The anatomic sites of the different levels are indicated by brightened lines on the videoroentgenographic projection image of the urethane cast on the left. At the upper level both epicardial and endocardial surfaces

are coincidentally uniform and nearly perpendicular to the scan plane. For this reason accuracy of the 0.3 mm thick and the 10.2 mm thick slices are very similar at this level.

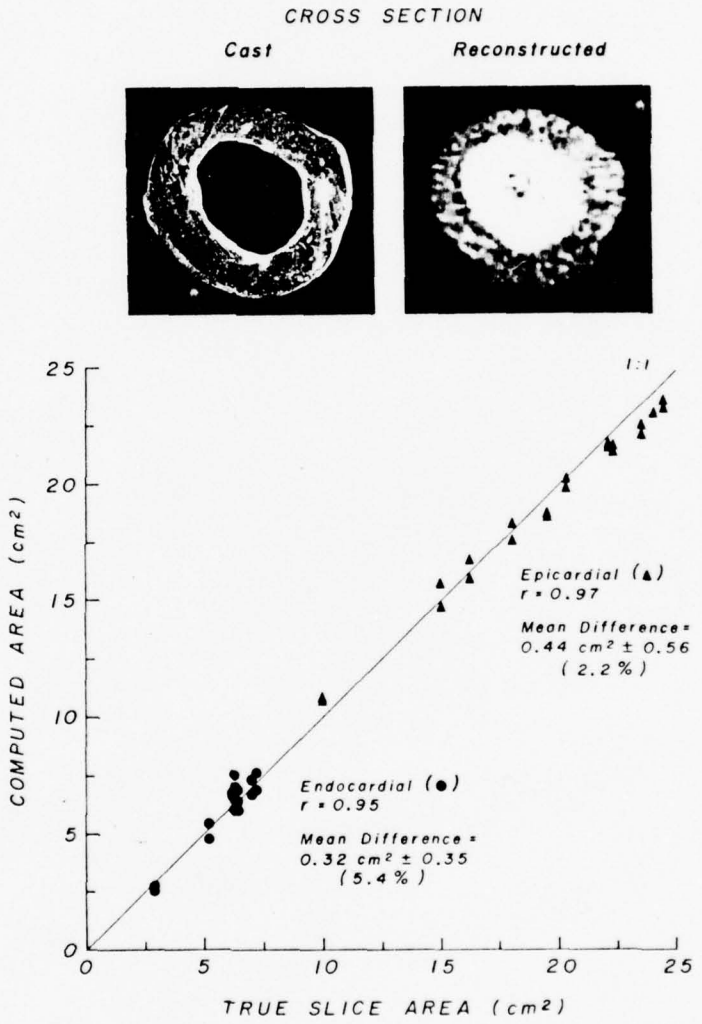

Figure 31 Comparison of actual and reconstructed cross-sectional images of urethane cast of left ventricle (top) and of epi- and endocardial areas of actual and reconstructed cross sections of cast determined for 21 levels from base-to-apex (bottom).

BEST AVAILABLE COPY

BEST AVAILABLE COPY

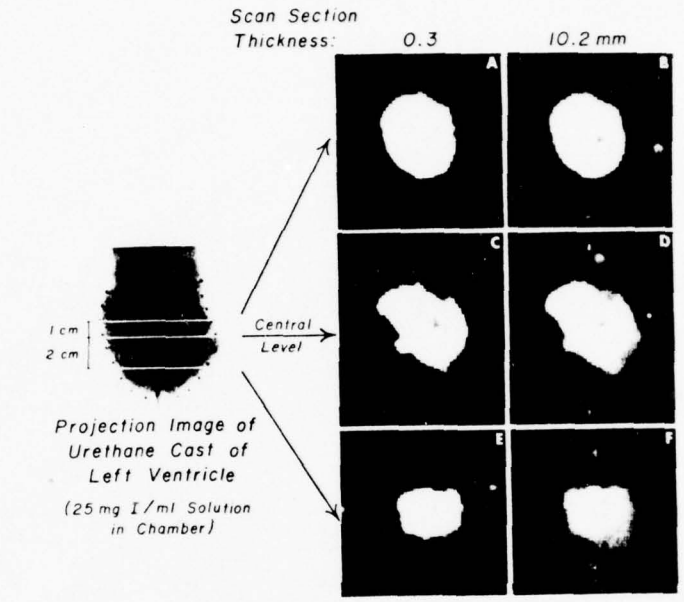

Figure 32 X-ray video projection image of urethane cast of left ventricle with three superimposed brightened lines at levels selected for cross-sectional reconstruction (left) and two sets of reconstructed cross-sectional images determined at these three levels for scan thickness of 0.3 mm and 10.2 mm, respectively (right).

However, at the central level the epicardial border becomes less distinct in the thicker 10.2 mm slice. This effect is most noticeable in the lower right and upper central segments of the endocardial surface. Also the difference between the position of the endocardial border in the lower right quadrant of the 0.3 mm and 10.2 mm thick slices is most marked, with the difference approximating one-half the wall thickness. In the region 20 mm below the central plane both the epicardial and endocardial surfaces are not

perpendicular to the scan plane. Therefore, the axial projection of a thick, 10.2 mm and a thin, 0.3 mm slice differ significantly at this level. The endocardial border in the 10.2 mm thick section is considerably "out of focus," making determination of the true shape and dimensions of the left ventricular model at this level impossible when using such a thick scan plane.

These results are particularly important for cross-sectional imaging of the heart in the intact chest since the base-to-apex axis of the ventricles is normally at an oblique angle to the long axis of the body which would conventionally be perpendicular to the scanning plane(s) of a computerized tomographic scanner. Hence, the epicardial and endocardial surfaces of the heart will usually not be perpendicular to the plane of reconstruction, further requiring that transaxial reconstruction slices be as thin as possible (1 mm) to permit accurate measurements of the shape and dimensions of the heart. In addition, simultaneous multiple parallel cross sections are needed to determine the true three-dimensional shape and dimensions of a moving organ such as the heart.

To study the effect in reconstructed images due to motion of the object during the circumferential scanning procedure, a mathematical test object was contrived. The simulated test object was a cylinder 7.62 cm in diameter with groups of one, two, four, and eight millimeter triangular serrations (to simulate trabeculae carnae and papillary muscles) inserted at 90° intervals around the perimeter.

Parallel projection data was mathematically generated for the simulated test object at equiangular increments of 1.8° over a range of 180°. Random quantum noise to simulate the photon statistics of the SSDSR was introduced into the projection data assuming an incident x-ray count of 10^5 x-ray photons per sampled ray (16). These mathematically derived projection data were used to reconstruct the test object shown in panel A of Figure 33 using a parallel

convolution algorithm with a 150 x 150 picture element matrix (pixel size of 0.7 mm x 0.7 mm). The 8 mm (upper right quadrant of Panel A), 4 mm (upper left quadrant), and 2 mm (lower left quadrant) serrations are all clearly visualized in this reconstruction. The location of the 1 mm serrations (lower right quadrant) can just be seen but the serrations cannot be separated, probably because the pixel size of the reconstruction is nearly the same as the size of the serrations.

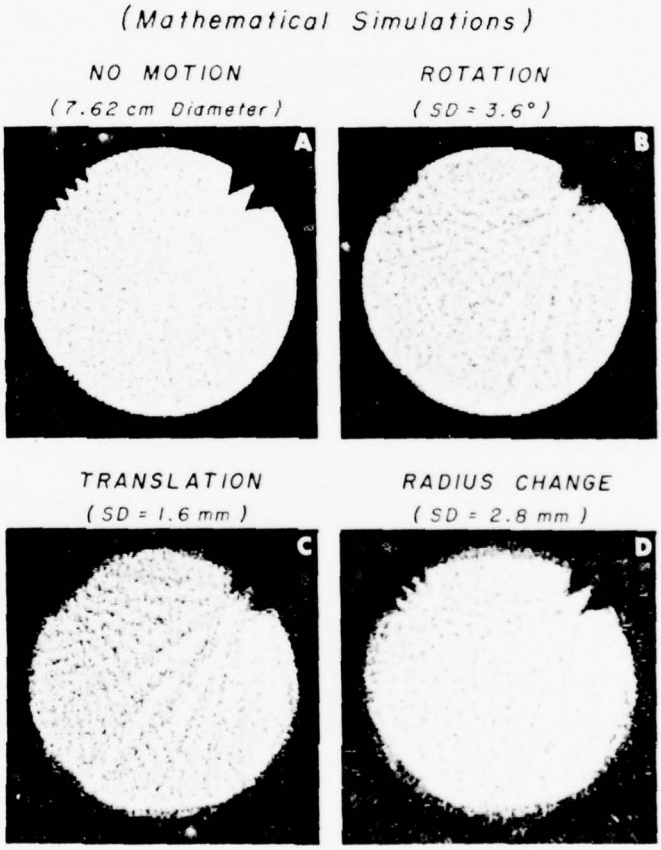

Figure 33 Reconstructed images of simulated cylindrical test object showing artifacts caused by motion during the scanning procedure. Mathematically derived projection data of the simulated 7.62 cm diameter plexiglass cylinder with 8, 2, 4, and 1 mm triangular serrations in equispaced groups around the perimeter were used to obtain reconstructions without motion (panel A), with rotational motion (panel B), with translation motion (panel C), and radial motion (panel D).

This image (panel A) reconstructed from mathematically accurate projection data serves as a reference against which the other images in the montage can be compared for image degradation due to motion. The effect of a random rotation around the center of the cylinder (as occurs in the heart during certain phases of the cardiac cycle) during the scanning procedure is illustrated in panel B. This effect was achieved by substituting, at each angle of view, mathematically derived projection data randomly selected to be at a greater, identical, or a lesser angle of view than the correct angle. The random variations in the angle of view at each viewing position were normally distributed with a mean of zero and a standard deviation of 3.6° resulting in a movement of up to 2 mm at the periphery of the cylinder. The smooth round perimeter of the reconstructed test object is very well defined as would be expected with motion tangential to this surface. However, the 2 mm and 4 mm serrations are obliterated and a faint shadow of the 8 mm serration is just visible. With no prior knowledge of the shape of the structure in this region, a true determination of the dimensions of the cylinder would be difficult.

The effect of random two-dimensional translational movements (as occur during asynchronous respiratory and cardiac cycles) of the cylinder in the plane of the reconstruction is illustrated in panel C of Figure 33. This effect was achieved by randomly shifting the projection data at each angle of view. The random shift was normally distributed with a mean of zero and a standard deviation of 1.6 mm. This caused a significant loss of definition of the smooth surface of the cylinder and failure to reproduce the 2 mm and 4 mm serrations.

The effects of random radius changes (to simulate slight changes in ventricular volume during breath holding or due to slight sinus arrhythmia), is shown in panel D. This effect was achieved by compressing or expanding the projection data with scaling about the center point. The magnitude of the radius change was normally distributed with a mean of zero and a standard deviation of 2.8 mm.

There is a significant loss of definition of the smooth boundary in the reconstructed image although the 8 mm serrations are clearly visible. The 4 mm serrations can be detected but are not well defined.

These studies of thickness and motion artifacts in reconstructed cross-sectional images using actual and simulated test objects indicate that the single or dual slice scan mode of all currently available commercial scanners coupled with their poor temporal resolution severely limit the application of these scanners to the study of the structure and function of moving organ systems such as the heart, lungs and circulation. Even if adequate single cross-sectional images can be generated using gating techniques, the difficulties associated with accurate positioning of the scanner at multiple parallel levels in relation to the organs under study, especially the heart, will be difficult to overcome because of motion of the subject or motion of the internal organs of the body. For these reasons, high temporal and axial resolution synchronous cylindrical scanning is practically a mandatory requirement for accurate studies of the structure and function of the dynamic organs of the body (22,25).

Summary and Significance (Part II)

The development in our laboratory of a single source computerized x-ray fluoroscopic system (i.e., SSDSR) for three-dimensional reconstruction and display of moving organs, particularly the heart, lungs and circulation, provides the potential for studies in intact animals and humans of the dynamic anatomy and associated functions of moving organs in ways never before achievable. This is because up until the development of computerized transaxial tomography there was no technique capable of accurate determination of the true shape and dimensions of these organs in intact animals

and humans. Three-dimensional reconstruction techniques can be applied to intact animals and humans in a variety of postures (e.g., prone, supine, right and left lateral decubitus positions) and under conditions of increased gravitational-inertial stress for heretofore impossible investigations of the relationships of the dynamic three-dimensional structural geometry to the physical and biochemical functions of both moving and stationary organ systems.

Earl H. Wood, M.D.,Ph.D.
Project Director

Peter A. Chevalier, Ph.D.
Principal Investigator

August 30, 1976

References

1. Wohl, M. E. B., J. Turner, and J. Mead:
Static volume-pressure curves of dog lungs - in vivo and in vitro.
J Appl Physiol 24:348-354, 1968.

2. Milic-Emili, J.:
Pulmonary statics.
Respiratory Physiology, J. G. Widdicombe, ed., Butterworths, London, 1974.

3. Milic-Emili, J., J. A. M. Henderson, M. B. Dolovich, and K. Kaneko:
Regional distribution of inspired gas in the lung.
J Appl Physiol 21:749-759, 1966.

4. Kaneko, K., J. Milic-Emili, M. B. Dolovich, A. Dawson, and D. V. Bates:
Regional distribution of ventilation and perfusion as a function of body position.
J Appl Physiol 21:767-777, 1966.

5. Smith, H. C., J. F. Greenleaf, E. H. Wood, D. J. Sass, and A. A. Bove:
Measurement of regional pulmonary parenchymal movement in dogs.
J Appl Physiol 34:544-547, 1973.

6. Chevalier, P. A., J. F. Greenleaf, R. A. Robb, and E. H. Wood:
Biplane videoroentgenographic analysis of dynamic regional lung strains in dogs.
J Appl Physiol 40:118-122, 1976.

7. Williams, J. P., R. E. Sturm, A. G. Tsakiris, and E. H. Wood:
Biplane videoangiography.
J Appl Physiol 24:724-727, 1968.

8. Sturm, R. E., E. L. Ritman, R. J. Hansen, and E. H. Wood:
Recording of multichannel analog data and video images on the same videotape or disc.
J Appl Physiol 36:761-764, 1974.

9. West, J. B., and F. L. Matthews:
Stresses, strains and surface pressures in the lung caused by its weight.
J Appl Physiol 32:332-345, 1972.

10. Milic-Emili, J., J. Mead, J. M. Turner, and E. M. Glauser:
Improved technique for estimating pleural pressure from esophageal balloons.
J Appl Physiol 19:207-211, 1964.

11. Gillespie, D. J., Y. L. Lai, and R. E. Hyatt:
Comparison of esophageal and pleural pressures in the anesthetized dog.
J Appl Physiol 35:709-713, 1973.

12. Robb, R. A., S. A. Johnson, J. F. Greenleaf, M. Wondrow, and E. H. Wood:
An operator-interactive, computer-controlled system for high fidelity digitization and analysis of biomedical images.
Proceedings, Society of Photo-optical Instrumentation Engineers 40:11-26, 1973.

13. Herman, G. T.:
A relaxation method for reconstructing objects from noisy x-rays.
Mathematical Programming 8:1-19, 1975.

14. Gordon, R., and G. T. Herman:
Three-dimensional reconstruction from projections: A review of algorithms.
In: International Review of Cytology, Vol. 38:111-151 (editors: G. H. Bourne and J. F. Danielli) Academic Press, New York, 1974.

15. Herman, G. T., S. A. Johnson, A. V. Lakshminarayanan, A. Lent, E. L. Ritman, R. A. Robb, S. W. Rowland, and E. H. Wood:
An algorithm for on-line, real-time reconstruction of the intact heart.
Computers in Cardiology Conference, October 2-4, 1975, Thoracentrum, Rotterdam, Netherlands (in press).

16. Sturm, R. E., E. L. Ritman, S. A. Johnson, M. A. Wondrow, D. I. Erdman, and E. H. Wood:
Prototype of a single x-ray video imaging chain designed for high temporal resolution computerized tomography by means of an electronic scanning dynamic spatial reconstruction system.
Proceedings, San Diego Biomedical Symposium, 15:181-188, 1976.

17. Ritman, E. L., S. A. Johnson, R. E. Sturm, and E. H. Wood:
The television camera in dynamic videoangiography.
Radiology 107:417-427, May, 1973.

18. Herman, G. T., A. Lent, and S. Rowland:
ART: Mathematics and applications (a report on the mathematical foundations and on the applicability to real data of the algebraic reconstruction techniques).
J Theor Biol 42:1-32, 1973.

19. Heethaar, R. M., R. A. Robb, Y. C. Pao, and E. L. Ritman:
Three-dimensional stress and strain analysis in the intact heart.
Proceedings, San Diego Biomedical Symposium, 15:337-342, 1976.

20. Ritman, E. L., R. E. Sturm, E. H. Wood:
Needs, performance requirements and proposed design of spatial reconstruction system for diagnostic and investigative studies of cardiopulmonary and circulatory dynamics.
In: Reconstructive Tomography in Diagnostic Radiology and Nuclear Medicine (editors: M. M. Ter-Pogossian, M. E. Phelps, G. L. Brownell, J. R. Cox, Jr., D. O. Davis, and R. G. Evens) University Park Press, Baltimore, 1976 (in press).

21. Herman, G. T., and H. K. Liu:
Detection and display of organ surfaces from computed tomograms.
Presented at the International Symposium and Course on Computerized Tomography, San Juan, Puerto Rico, April 5-9, 1976.

22. McCullough, E. C., H. L. Baker, O. W. Houser, and D. F. Reese:
An evaluation of the quantitative and radiation features of a scanning x-ray transverse axial tomograph: The EMI scanner.
Radiology 111:709-715, 1974.

23. Harris, L. D., R. A. Robb, E. H. Wood, and E. L. Ritman:
Measurement of left ventricular wall thickness and chamber volume using three-dimensional reconstruction.
The Physiologist 18:240, 1975.

24. Robb, R. A., J. F. Greenleaf, E. L. Ritman, S. A. Johnson, J. Sjostrand, G. T. Herman, and E. H. Wood:
Three-dimensional visualization of the intact thorax and contents: A technique for cross-sectional reconstruction from multiplanar x-ray views.
Computers and Biomedical Research 7:395-419, 1974.

25. Wood, E. H.:
Cardiovascular and pulmonary dynamics by quantitative imaging.
Circ Res 38:131-139, 1976.

PART III: Publications From This Laboratory Based on Work Performed Under, and Supported By, This Contract (AF-44620-71-C-0069) For the Years 1971-1976

All of the following publications acknowledge the support provided by this contract and the U.S. Air Force. Copies (3) of papers published during the past year (1975-1976) are included with this progress report. Copies of papers "in press" and "in manuscript" will be forwarded upon receipt of reprints.

1. Greenleaf, J. F., H. C. Smith, A. A. Bove, D. J. Sass, and E. H. Wood:
   EFFECT OF CHANGES IN THE MAGNITUDE AND DIRECTION OF THE FORCE ENVIRONMENT OF REGIONAL DISTORTION OF LUNG PARENCHYMA IN DOGS
   The Physiologist 14:155 (August) 1971 Abstract

2. Sass, D. J., J. F. Greenleaf, H. C. Smith, A. A. Bove, and E. H. Wood:
   EFFECTS OF ACCELERATION ON PULMONARY BLOOD FLOW IN DOGS BREATHING ORGANIC LIQUIDS
   The Physiologist 14:223 (August) 1971 Abstract

3. Coulam, C. M. and E. H. Wood:
   REGIONAL DIFFERENCES IN PLEURAL AND ESOPHAGEAL PRESSURES IN HEAD-UP AND HEAD-DOWN POSITIONS
   Journal of Applied Physiology 31:277-287 (August) 1971

4. Sass, D. J., E. L. Ritman, P. E. Caskey, W. VanNorman, and E. H. Wood:
   RESPIRATORY VARIATIONS IN LEFT VENTRICULAR STROKE VOLUME DURING LIQUID BREATHING
   Proceedings, Aerospace Medical Association Annual Scientific Meeting, 1971.

5. Greenleaf, J. F., C. M. Coulam, W. Dunnette, and E. H. Wood:
   COMPUTER ACQUISITION, ANALYSIS AND DISPLAY OF SCINTISCANNER DATA FOR DETERMINATION OF THE SPATIAL DISTRIBUTION OF BLOOD FLOW: HARDWARE
   Proceedings of Symposium on Sharing of Computer Programs and Technology in Nuclear Medicine, Oak Ridge, Tennessee, April 2-3, 1971, pp 61-65

6. Greenleaf, J. F., C. M. Coulam, W. Dunnette, and E. H. Wood:
COMPUTER ACQUISITION, ANALYSIS AND DISPLAY OF SCINTISCANNER DATA FOR DETERMINATION OF THE SPATIAL DISTRIBUTION OF BLOOD FLOW: SOFTWARE
Ibid, pp 67-83

7. Sass, D. J., J. F. Greenleaf, P. E. Caskey, E. L. Ritman, S. A. Johnson, H. F. Helmholz, Jr. (and E. H. Wood):
BLOOD pH IN DOGS BREATHING OXYGENATED FC 80 FLUOROCARBON
Federation Proceedings 31:348 (March-April) 1972 Abstract

8. Sass, D. J., E. L. Ritman, P. E. Caskey, N. Banchero, and E. H. Wood:
LIQUID BREATHING: PREVENTION OF PULMONARY ARTERIAL-VENOUS SHUNTING DURING ACCELERATION
Journal of Applied Physiology 32:451-455 (April) 1972

9. Coulam, C. M., J. F. Greenleaf, A. G. Tsakiris, and E. H. Wood:
THREE-DIMENSIONAL COMPUTERIZED DISPLAY OF PHYSIOLOGIC MODELS AND DATA
Computers and Biomedical Research 5:166-179, 1972

10. Sass, D. J., W. Van Norman, E. H. Wood, and S. Zahn:
DIGITAL COMPUTER ANALYSIS OF CIRCULATORY AND RESPIRATORY PRESSURES IN WATER-IMMERSED DOGS BREATHING LIQUID IN FORCE ENVIRONMENTS OF 1 and 7Gy
Aerospace Medical Association Preprint, 1972 Annual Scientific Meeting May 8-11, 1972, Bal Harbour, Florida, pp 242,243

11. Greenleaf, J. F., H. C. Smith, D. J. Sass, E. L. Ritman, and E. H. Wood:
REGIONAL DISTRIBUTION OF BLOOD FLOW IN THE LUNGS OF DOGS IN LEFT DECUBITUS POSITION
Physiologist 15:153 (August) 1972 Abstract

12. Sass, D. J., J. F. Greenleaf, E. L. Ritman, and E. H. Wood:
SOME CARDIOPULMONARY EFFECTS OF LIQUID BREATHING DURING CHANGES IN THE FORCE ENVIRONMENT
Proceedings of the Fifth Symposium on Underwater Physiology, August 21-25, 1972, Freeport, British Bahamas, sponsored by the University of Pennsylvania and Undersea Medical Society, p 122 Abstract

13. Smith, H. C., J. F. Greenleaf, E. H. Wood, D. J. Sass, and A. A. Bove:
MEASUREMENT OF REGIONAL PULMONARY PARENCHYMAL MOVEMENT IN DOGS
Journal of Applied Physiology 34:544-547 (April) 1973

14. Sass, D. J., A. C. Nolan, and E. H. Wood:
DIGITAL COMPUTER ANALYSIS OF CIRCULATORY AND RESPIRATORY PRESSURES IN WATER-IMMERSED DOGS BREATHING LIQUID IN FORCE ENVIRONMENTS OF 1 AND 7 Gy
Aerospace Medicine 45:1-11 (January) 1974

15. Chevalier, P. A., J. F. Greenleaf, R. A. Robb, and E. H. Wood:
BIPLANE VIDEOROENTGENOGRAPHIC ANALYSIS OF DYNAMIC REGIONAL LUNG STRAINS IN DOGS
The Physiologist 17:195 (August) 1974 Abstract

16. Greenleaf, J. F., E. L. Ritman, D. J. Sass, and E. H. Wood:
SPATIAL DISTRIBUTION OF PULMONARY BLOOD FLOW IN DOGS IN LEFT DECUBITUS POSITION
Amer J Physiol 227:230-244, 1974

17. Sturm, R. E., E. L. Ritman, and E. H. Wood:
QUANTITATIVE THREE-DIMENSIONAL DYNAMIC IMAGING OF STRUCTURE AND FUNCTION OF THE CARDIOPULMONARY AND CIRCULATORY SYSTEMS IN ALL REGIONS OF THE BODY
In: Cardiovascular Imaging and Image Processing, Vol. 72, (Editors: D. C. Harrison, H. Sandler, H. A. Miller), 1975, pp 103-122

18. Robb, R., Ritman, E., and E. H. Wood:
THREE-DIMENSIONAL RECONSTRUCTION AND DISPLAY OF THE HEART, LUNGS AND CIRCULATION BY MULTIPLANAR X-RAY SCANNING VIDEO-DENSITOMETRY
Ibid. pp 183-194

19. Smith, H. C., R. A. Robb, and E. H. Wood:
MYOCARDIAL BLOOD FLOW: ROENTGEN VIDEODENSITOMETRY TECHNIQUES
Ibid. pp 225-232

20. Greenleaf, J. F., S. A. Johnson, W. F. Samayoa, and F. A. Duck:
ALGEBRAIC RECONSTRUCTION OF SPATIAL DISTRIBUTION OF ACOUSTIC VELOCITIES IN TISSUE FROM THEIR TIME OF FLIGHT PROFILES
In: Acoustical Holography, Volume 6:71-90 (Newell Booth, editor) Plenum Press, New York, 1975

21. Chevalier, P. A., L. D. Harris, J. F. Greenleaf, and R. A. Robb:
DYNAMIC REGIONAL LUNG STRAINS IN AWAKE DOGS
The Physiologist 18:168 (August) 1975 Abstract

22. Ino-Oka, E., L. D. Harris, P. A. Chevalier, and E. L. Ritman:
LEFT VENTRICULAR MYOCARDIAL FIBER ANGLE DYNAMICS
The Physiologist 18:259 (August) 1975 Abstract

23. Greenleaf, J. F., S. A. Johnson, W. F. Samayoa, and F. A. Duck:
RECONSTRUCTION OF SPATIAL DISTRIBUTIONS OF REFRACTION INDICES IN TISSUE FROM TIME-OF-FLIGHT PROFILES
Image Processing for 2-D and 3-D Reconstruction from Projections: Theory and Practice in Medicine and the Physical Sciences. A Digest of Technical Papers. August 4-7, 1975, Stanford, California, pp MA2-1 - MA2-4.

24. Wood, E. H., D. J. Sass, J. F. Greenleaf, H. C. Smith, and E. L. Ritman:
SOME EFFECTS OF CHANGES IN THE GRAVITATIONAL-INERTIAL FORCE ENVIRONMENT ON THE HEART AND LUNGS.
Man in Space (Proceedings, 4th International Symposium on Basic Problems of Man's Life in Cosmic Space), Erevan (Armenia) 1-6 October 1971 (editors: O. G. Gazenko and H. Bjurstedt), publisher, Science, Moscow, 1974, pp 91-124.

25. Chevalier, P. A., J. F. Greenleaf, R. A. Robb, and E. H. Wood:
BIPLANE VIDEOROENTGENOGRAPHIC ANALYSIS OF DYNAMIC REGIONAL LUNG STRAINS IN DOGS
Journal of Applied Physiology 40:118-122 (January) 1976

26. Wood, E. H.:
NEW HORIZONS FOR STUDY OF THE CARDIOPULMONARY AND CIRCULATORY SYSTEM
Chest 69:394-408 (March) 1976

27. Wood, E. H.:
CARDIOVASCULAR AND PULMONARY DYNAMICS BY QUANTITATIVE IMAGING
Circulation Research 38:131-139 (March) 1976

28. Chevalier, P. A., L. D. Harris, R. A. Robb, J. F. Greenleaf, and E. H. Wood:
THREE-DIMENSIONAL RECONSTRUCTION OF THE HEART AND LUNGS BY MULTIPLANAR X-RAY SCANNING VIDEODENSITOMETRY
Proceedings, Aerospace Medical Association Annual Scientific Meeting, Bal Harbour, Florida, May 10-13, 1976, pp 237-238

29. Sass, D. J., R. A. Van Dyke, E. H. Wood, S. A. Johnson, and P. Didisheim:
GAS EMBOLISM DUE TO INTRAVENOUS FC 80 LIQUID FLUOROCARBON
Journal of Applied Physiology 40:745-751 (May) 1976

30. Robb, R. A., E. L. Ritman, J. F. Greenleaf, R. E. Sturm, G. T. Herman, P. A. Chevalier, H. K. Liu, and E. H. Wood:
QUANTITATIVE IMAGING OF DYNAMIC STRUCTURE AND FUNCTION OF THE HEART, LUNGS AND CIRCULATION BY COMPUTERIZED RECONSTRUCTION AND SUBTRACTION TECHNIQUES
Proceedings, Third Annual Conference on Computer Graphics, (SIGGRAPH), July 14-16, 1976 (in press)

31. Robb, R. A., E. L. Ritman, R. E. Sturm, G. T. Herman, and E. H. Wood:
DYNAMIC THREE-DIMENSIONAL RECONSTRUCTION OF THE CARDIOPULMONARY SYSTEM AND CIRCULATION
Proceedings of the 61st Scientific Assembly and Annual Meeting of the Radiological Society of North America, December 1-5, 1975, Chicago, Illinois, 1976 (in press)

32. Johnson, S. A., R. A. Robb, E. L. Ritman, B. K. Gilbert, J. F. Greenleaf, L. D. Harris, M. J. Berggren, R. E. Sturm, P. A. Chevalier, R. M. Heethaar, E. H. Wood, G. T. Herman, and Y. C. Pao:
BIOIMAGE SYNTHESIS AND ANALYSIS FROM X-RAY, GAMMA, OPTICAL, AND ULTRASOUND ENERGY
In: Digital Processing of Biomedical Images, Proceedings of 1975 United States-Japan Seminar, October 27-31, Pasadena, California, 1976 (in press)

33. Ritman, E. L., H. C. Smith, R. A. Robb, R. E. Sturm, and E. H. Wood:
ROENTGEN VIDEODENSITOMETRY AND VIDEO SCANNING DENSITOMETRY APPLICATION TO THE CARDIOVASCULAR SYSTEM
Chapter in Cardiac Radiology (Editor: Dr. Erik Carlsson) 1976 (in press).

34. Gilbert, B. K., M. T. Storma, C. E. James, L. W. Hobrock, E. S. Yang, K. C. Ballard, and E. H. Wood:
A REAL-TIME HARDWARE SYSTEM FOR DIGITAL PROCESSING OF WIDEBAND VIDEO IMAGES
IEEE Transactions on Computers, 1976 (in press)

35. Gilbert, B. K., M. T. Storma, K. C. Ballard, L. W. Hobrock, C. E. James, and E. H. Wood:
A PROGRAMMABLE DYNAMIC MEMORY ALLOCATION SYSTEM FOR INPUT OUTPUT OF DIGITAL DATA INTO STANDARD COMPUTER MEMORIES AT 40 MEGASAMPLES/S
IEEE Transactions on Computers, 1976 (in press)

36. Gilbert, B. K., W. F. Sutterer, J. J. Tiemann, S. A. Johnson, R. D. Baertsch, R. E. Sturm, and E. H. Wood:
A CHARGE COUPLED TRANSVERSAL FILTER FOR BIOMEDICAL SIGNAL CONDITIONING
Proceedings of the Joint Thirteenth Annual Rocky Mountain Bioengineering Symposium and Thirteenth International ISA Biomedical Sciences, Instrumentation Symposium, University of Wyoming, May 3-5, 1976 (in press)

37. Johnson, S. A., J. F. Greenleaf, R. C. Bahn, W. F. Samayoa, F. Duck, C. Hansen, M. Tanaka, and A. Lent:
RECONSTRUCTION OF THREE-DIMENSIONAL ULTRASOUND TISSUE PROPERTIES FROM TRANSMISSION AND OTHER DATA
American College of Radiology Conference on Computerized Tomography in Radiology, St. Louis, Missouri, April 25-28, 1976

38. Wood, E. H. and E. L. Ritman:
ZERO REFERENCE AND CALIBRATION PROBLEMS OF CIRCULATORY PRESSURES RECORDED BY IMPLANTED AND INDWELLING PRESSURE TRANSDUCERS, AND A LOOK AT FUTURE TECHNOLOGY FOR STUDIES OF DYNAMIC RELATIONSHIPS OF STRUCTURE TO FUNCTION OF THE HEART, LUNGS, AND CIRCULATION
In: Indwelling Pressure Transducers (CRC Press, Inc., Cleveland, Ohio, 1976 (in press)

39. Wood, E. H.:
THE EFFECTS OF TRANSVERSE ACCELERATION ON CHIMPANZEES
Proceedings of the "Use of Non-Human Primates in Space," NASA Ames Research Center, December 4, 1974 (in press)

40. Ritman, E. L., R. E. Sturm, R. A. Robb, and E. H. Wood:
NEEDS, REQUIREMENTS AND DESIGN OF A HIGH TEMPORAL RESOLUTION SYNCHRONOUS CYLINDRICAL WHOLE-BODY TRANSAXIAL SCANNER FOR SIMULTANEOUS STUDY OF THE STRUCTURE AND FUNCTION OF THE HEART AND CIRCULATION
In: Roentgen Video Techniques for Dynamic Studies of Structure and Functions. Editor: Prof. P. Heintzen, G. Thieme, Stuttgart, 1976 (in press).

41. Sturm, R. E., E. L. Ritman, and E. H. Wood:
PROTOTYPE OF A SINGLE X-RAY VIDEO IMAGING CHAIN DESIGNED FOR A FULLY ELECTRONIC, SYNCHRONOUS CYLINDRICAL SCANNING, DYNAMIC SPATIAL RECONSTRUCTION SYSTEM
Ibid.

42. Wood, E. H. and E. L. Ritman:
CURRENT CAT SCANNERS IN RELATION TO THE NEEDS AND REQUIREMENTS FOR A NEW GENERATION HIGH TEMPORAL RESOLUTION AND HIGH SYNCHRONOUS AXIAL ANATOMIC RANGE AND RESOLUTION DYNAMIC SPATIAL RECONSTRUCTION SYSTEM FOR SIMULTANEOUS STUDY OF STRUCTURE AND FUNCTIONS OF THE HEART AND CIRCULATION
Ibid.

43. Gilbert, B. K., A. Chu, and E. L. Ritman:
DATA MANAGEMENT, COMPUTATION, AND DISPLAY TECHNIQUES FOR DYNAMIC SPATIAL RECONSTRUCTION OF STRUCTURAL AND FUNCTIONAL INFORMATION FROM THE HEART, LUNGS AND CIRCULATORY SYSTEM
Ibid.

44. Robb, R. A., L. D. Harris, P. A. Chevalier, and E. L. Ritman:
QUANTITATIVE DYNAMIC THREE-DIMENSIONAL IMAGING OF THE HEART AND LUNGS BY COMPUTERIZED SYNCHRONOUS CYLINDRICAL SCANNING RECONSTRUCTION TOMOGRAPHY
Ibid.

45. Ruegsegger, P. E., L. D. Harris, S. W. Rowland, and E. L. Ritman:
PREDICTIONS OF THE PERFORMANCE OF A DYNAMIC SPATIAL RECONSTRUCTION SYSTEM BASED ON MATHEMATICAL SIMULATIONS
Ibid.

46. Harris, L. D., P. Ruegsegger, and E. L. Ritman:
COMPUTERIZED TRANSAXIAL CROSS-SECTIONAL AND CYLINDRICAL SCANNING OF THE STRUCTURE AND FUNCTION OF DYNAMIC ORGANS - THE ROLE OF SPATIAL AND TEMPORAL RESOLUTION
Ibid.

47. Smith, H. C., R. A. Robb, and E. L. Ritman:
ROENTGEN VIDEODENSITOMETRIC ASSESSMENT OF MYOCARDIAL BLOOD FLOW: CLINICAL APPLICATIONS
Ibid.

48. Robb, R. A., E. L. Ritman, L. D. Harris, and P. A. Chevalier:
DYNAMIC SPATIAL RECONSTRUCTION TOMOGRAPHY FOR QUANTITATIVE STUDIES OF STRUCTURE AND FUNCTION OF THE HEART, LUNGS AND CIRCULATION
In: Computerized Three-Dimensional Reconstructions of Structure and Function (Symposium) Federation Proceedings, 1976 (in press)

49. Ritman, E. L., R. E. Sturm, R. A. Robb, and E. H. Wood:
QUANTITATIVE TRANSAXIAL IMAGING OF CARDIOVASCULAR SYSTEM - NEEDS, REQUIREMENTS AND IMPLEMENTATION
Ibid.

50. Wood, E. H., L. D. Harris, and P. E. Ruegsegger:
COMPUTERIZED THREE-DIMENSIONAL RECONSTRUCTION OF STRUCTURE AND FUNCTION OF BIOLOGIC OBJECTS
Ibid.

51. Chevalier, P. A., R. A. Robb, J. F. Greenleaf, L. D. Harris, and E. H. Wood:
DYNAMIC MEASUREMENTS OF REGIONAL LUNG STRAINS AND VOLUMES IN THE INTACT THORAX BY COMPUTER ANALYSIS OF BIPLANE ROENTGEN VIDEOGRAPHIC IMAGES
1976 (In Manuscript)

52. Greenleaf, J. F., E. L. Ritman, D. J. Sass, and E. H. Wood:
EFFECTS OF AN INCREASED FORCE ENVIRONMENT ON SPATIAL DISTRIBUTION OF PULMONARY BLOOD FLOW IN DOGS
1976 (In Manuscript)

53. Robb, R. A., L. D. Harris, and E. L. Ritman:
COMPUTERIZED X-RAY RECONSTRUCTION TOMOGRAPHY IN STEREOMETRIC ANALYSIS OF CARDIOVASCULAR DYNAMICS
Proceedings, 20th Annual Technical Symposium, SPIE, San Diego, California, August 23-27, 1976 (in press)

54. Wood, E. H., E. L. Ritman, L. D. Harris, and P. E. Ruegsegger:
NEW VISTAS FOR STUDIES OF STRUCTURAL AND FUNCTIONAL DYNAMICS OF THE HEART, LUNGS AND CIRCULATION BY QUANTITATIVE IMAGING
Proceedings, Conference on Diagnostic Imaging, Chicago, Illinois, September 27-28, 1976 (in press)

55. Johnson, S. A., E. L. Ritman, and E. H. Wood:
A UNIQUE BIOIMAGE SYNTHESIS AND ANALYSIS FACILITY AT MAYO CLINIC
Proceedings, IEEE Systems, Man and Cybernetics Society Meeting, November 8-13, 1976 (in press)

Appendix

PROTOTYPE OF A SINGLE X-RAY VIDEO IMAGING CHAIN DESIGNED FOR A FULLY ELECTRONIC, SYNCHRONOUS CYLINDRICAL SCANNING, DYNAMIC SPATIAL RECONSTRUCTION SYSTEM

Ralph E. Sturm

Erik L. Ritman, M.D., Ph.D.

Earl H. Wood, M.D., Ph.D.

Biophysical Sciences Unit, Mayo Clinic and Mayo Foundation, Mayo Graduate School of Medicine, Rochester, Minnesota

These investigations were supported in part by Research Grants HL 04664 and RR-7 from the National Institutes of Health, U. S. Public Health Service; NGR 24-003-001 from the National Aeronautics and Space Administration, AF 44620-71-C-0069, Office of Research of the United States Air Force.

Dr. Wood is a Career Investigator of the American Heart Association.

INTRODUCTION

The three-dimensional anatomic distribution of tissues of differing densities within the human body can be visualized by generating images of multiple parallel cross sections using the technique of computer-assisted synchronous cylindrical scanning tomography (Johnson, et al., 1974; Robb, et al., 1974). Existing computerized transaxial tomographic systems scan one or two cross sections at a time and have other operational restrictions which severely limit use for three-dimensional reconstruction of moving organs or structures, especially the heart, lungs and the circulation in all regions of the body. Primarily, these limitations (Robinson 1975) consist of the duration of scan required (generally greater than 5 seconds) per cross section imaged, thickness of the cross section (often greater than 10 mm) and need to mechanically move either the patient or the scanning assembly to image parallel cross sections. These constraints preclude effective "stop-action" (<0.01 sec) imaging of a three-dimensional volume containing a moving organ such as the heart, lungs, or flowing blood. Optimal reconstruction of the intact thorax requires imaging of its full anatomic axial and transverse extents. Consequently, the sets of x-ray projection "profiles" at each angle of view should cover an area of at least 30 x 30 cm to include all or a major portion of most chests. In addition and ideally, the roentgen density values of the projection images recorded at each angle of view should have adequate sensitivity and

signal-to-noise characteristics to permit discrimination of roentgen intensity differences caused by a change of x-ray beam attenuation of 0.1% or less (see Ritman, et al., this volume).

A prototype x-ray imaging system has been designed and fabricated to achieve the imaging specifications required for reconstruction of the three-dimensional distribution of roentgen densities within all or a major portion of the transverse and cephalocaudal extents of the thorax and at frequent intervals of time throughout individual respiratory and/or cardiac cycles. The system generates conventional roentgen video fluoroscopic images for direct visualization and recording as well as direct high fidelity on-line analog-to-digital conversion of a raster of up to 1000 discrete values covering the horizontal extent of each of a maximum of 250 lines per video field (Gilbert, et al., 1976; Robb, et al., 1973) at each "angle of view" around the subject. From these data up to 250 parallel adjacent cross-sectional images can be computed. The thickness and spacing interval of each cross section is about 0.4 and 0.9 mm, respectively, with a pixel resolution of 250 x 250 at each of the 250 levels (Johnson, et al., 1974).

Each of these 62,500 pixels defines a finite area element on the surface of each cross section. Since each cross section is of finite thickness, each pixel also represents a finite volume element, i.e., a voxel, in each cross section. The total three-dimensional

reconstructed array of voxel x-ray density values of, for example the entire thorax, provides the capability, without sequential scanning procedures, of computing sectional images with as many different orientations as desired in relation to the body axes (e.g., sagittal, coronal or other sectional orientations) in addition to the transaxial sections reconstructed from the original scan (Robb, et al., 1976)). The needs and requirements of an all electronic cylindrical scanning assembly to acquire all the necessary data within 0.01 sec and with a maximum repetition rate of 60 cylindrical scans per second have been described elsewhere (Ritman, et al., 1975).

METHOD

A schematic of the prototype imaging system is provided in Fig. 1. The x-ray pulses generated by a conventional rotating-anode x-ray tube either pass through the subject and are attenuated according to the integrated roentgen density through the subject or pass alongside the subject remaining essentially unattenuated. The resulting x-ray image is projected onto a 30 cm x 30 cm flat fluorescent screen after passing through a focused, 85 lines per mm 15:1, collimating grid. The fluorescent screen is of the gadolinium dioxysulphide terbium activated (Gd_2O_2S:Tb) type selected for low lag, low noise and high x-ray-to-light conversion efficiency. In addition, the light output is predominantly monochromatic at

approximately 540 nanometers which is particularly convenient in objective lens design.

g. 1

An f/0.95 50 mm focal length objective lens (f/0.75 50 mm lens will be utilized when it becomes available) is used to focus the fluorescent screen image onto the input photoelectric surface of a magnetically focused image intensifier. The objective lens minifies the image to produce a 28 x 28 mm image. In an assembly in which the objective lens and image intensifier are positioned at right angles to the fluorescent screen, a dichroic mirror was found to be the only suitable mirror. Optical coating of all objective lens surfaces was required to reduce scatter and maximize transmission. In addition the inner surface of the structural enclosure housing the objective lens and mirror had to be baffled with light traps and painted with highly absorbent paint (Nextel Velvet Coating, 3M) to reduce the noise produced by light reflected back from the enclosure onto the fluorescent screen.

The image intensifier amplifies light intensity by up to 50,000 times while maintaining a 1:1 magnification at the output phosphor. The two-stage magnetically focused system has a 1000:1 dynamic range and high signal-to-noise ratio (RCA Electro-Optics Handbook 1974). The very bright output image permitted the use of commercially available relay lenses for focusing the image with 1:1 magnification onto the photocathode of an image isocon television pickup tube with very little vignetting.

The image isocon (RCA Electro-Optics Handbook 1974) video camera was selected for its high sensitivity and dynamic range (1000) in order to match the dynamic range of the image intensifier. The image isocon operates in a 525 line, 60 field-per-second format. Additional favorable features are the low "lag" (Ritman, et al., 1973), low noise, ability to integrate the target for at least 2 seconds (normally 1/60 second) to increase the "sensitivity", to "zoom in" to smaller central portions of the image and to tolerate very bright portions within the image (due to "raw" beam passing alongside but not through the thorax) without loss of the dynamic range and signal-to-noise within the image of the thorax.

The image isocon device also has the ability to retain linearity in regions of the image illuminated at x-ray intensities which produce output signals below the "knee" of the characteristic brightness/signal output curve while simultaneously a portion of the x-ray image intensity exceeds the linearity range of the tube so that a portion of the scene is imaged beyond the normal operating range of the camera (see Fig. 6). This capability is particularly important because the full 1000:1 dynamic range of the imaging chain can be utilized for imaging the anatomic structure of interest (e.g., heart), when portions of the image generated by unattenuated "raw" x-ray beam image are intentionally allowed to exceed the "knee" of the characteristic curve of the imaging chain. This practice permits discrimination of x-ray intensity differences down to four orders of magnitude of the unattenuated "raw" beam and thereby correspondingly increases the potential density resolution of the cross-sectional image of the structure of interest. The reconstructed

images obtained from this type of scanning are subject to some distortion confined majorly to the region of structural borders at which very large changes in x-ray density occur (e.g., the external surfaces of the thorax) and which have no apparent significant effect on the quality of the reconstruction of internal structures (e.g., the heart). Successful methods for correction of this type of distortion have been implemented (Ruesgegger and Ritman, unpublished data).

Normally the video image is recorded on video tape, stop-action video disc or is converted directly from analog-to-digital form for storage in the computer (Robb, et al., 1973).

The efficiency of the imaging chain is depicted by tracing a single x-ray photon through the system as shown in Fig. 2. The absorption of the fluorescent screen is approximately 50% (Sturm and Morgan 1949) so that if two x-ray photons are incident on the screen only one will, on the average, be absorbed. If the x-ray continuous spectrum, i.e., the bremsstrahlung energy, is integrated and the photons are normalized to 70 kev photons, at normal fluoroscopic levels and x-ray to fluorescent screen distances, there would be approximately 2×10^7 photons per mm^2 incident on the anatomic structure per second.

ig. 2

One of these 70 kev photons absorbed by the screen would produce approximately 5,000 light photons (Sturm and Morgan 1949), of which 50% would be useful on the camera side of the screen. The efficiency of the specially coated objective lens, 50 mm focal length f/0.75 is 0.2%, therefore approximately 13.5 light photons would be projected onto the input photoelectric surface of the image-intensifier. The efficiency of this surface is 11% - so that, this one x-ray photon absorbed by the screen produces 1.4 photo electrons. Therefore,

this becomes the weakest link in the chain since from this point on, the photoelectrons are accelerated to impinge on a phosphor producing a large increase in light photons. In fact, this intensifier, together with the image-isocon, is normally used with a gain of more than 25,000 in equivalent light intensity.

What does this mean in terms of television system performance? Since each picture is viewed by the television camera target at 60 times (i.e., fields) per second, the x-rays in the raw beam (i.e., 2×10^7 per second per mm^2) in this unit is reduced to about 3.3×10^5 x-ray photon per field per mm^2 due to this short exposure time and the increased x-ray-to-subject distance as shown in Column A of Fig. 2. Since some regions of the thorax (i.e., the heart, spine, and chest walls) absorb practically 99% of this radiation, this reduces to 3.3×10^3 photons per field or exposure per mm^2 shown in Column B.

The number of photons imaged per unit area can be increased if the minimal area of interest is increased. Thus, by averaging the image signal from 4 adjacent video lines (lines about 1 mm apart) within the image approximately a two-fold increase of signal-to-noise (i.e., $\sqrt{4}$) can be achieved. The validity of this approach depends on the "independence" (i.e., statistical nature) of the noise in the image chain output signal.

The statistical nature of the imaging chain noise has been verified. Averaging of signal data samples, either taken at successive points in time from the same point in the image, or from contiguous regions in a uniform image obtained at one point in time, increases the signal-to-noise in proportion to the square root of the number of averaged data points. Fig. 3 illustrates this finding.

ig. 3

The ability to "drive" the raw, unattenuated x-ray beam portion of the image over the "knee" of the characteristic curve of the image isocon camera can be utilized to increase the signal in that section of the image that is of interest (e.g., the heart) by integrating images generated by sequential x-ray pulses on the camera tube target. This is accomplished by disabling the 60-per-second electronic sweep-off mechanism until an adequate signal has been accumulated. Fig. 4 illustrates how the video tube target integration time can be controlled via the computer. This approach effectively increases the radiation flux-per-image pixel while retaining normal x-ray radiation flux per pulse. This procedure reduces the number of images-per-second that can be recorded in direct proportion to the number of successive 60-per-second x-ray images integrated on the target. This technique has also been used to image the distribution of radioisotopes on the basis of their emitted radiation (Berggren, et al., 1976). Up to a ten-fold increase (relative to the radiation required in a small chest) in

x- or gamma-ray flux-per-image pixel may be necessary to adequately image the heart in a large chest. This will require up to 150 msec "integration" times between successive "read outs" of the isocon camera target.

ig. 4

RESULTS

a) Operational Characteristics

Due to the use of a flat fluorescent screen and flat photocathodes of the image intensifier and image isocon tubes, very little geometric distortion occurs over the entire field of view as shown in Fig. 5a. The lenses and image isocon systems, however, exhibit radial intensity fall-off as shown in the intensity plot of a single selected video line (brightened in image) as shown in panel c. The image brightness at the periphery is 80% of the brightness at the center. The dynamic range and signal-to-noise characteristics are illustrated in panels b and d.

ig. 5

The system input/output linearity is demonstrated in Fig. 6. In the presence of monochromatic x-ray and absence of imaged x-ray scatter, the Beer-Lambert law should be obeyed (Heintzen and Moldenhauer 1971) so that the logarithm of the image intensity should linearly decrease with increasing depth of water traversed by the x-ray beam.

ig. 6

Although operation of the imaging chain so that segments of the image exceed "the knee of the curve" as illustrated in curve II results in loss of some information (e.g., the outer chest wall) the resultant increase in ability to discriminate small changes in x-ray intensity within the regions of greatest interest makes improved roentgen density resolution within the cross-sectional images of these regions (e.g., the heart) possible. That operation of the image isocon video camera in the integrating mode provides an increase of the image pixel signal which relates directly to the number of pulsed x-ray images integrated is shown in Fig. 7. This linear relationship is maintained in the presence of "saturation" if the image signal in certain regions, such as when the raw beam is imaged alongside the chest.

ig. 7

b) Application of the System

A conventional projection image of a canine thorax and one selected (out of a possible 250) cross-sectional image computed from the projection images of the chest at 28 angles of view around 160° (Robb, et al., 1976) is shown in Fig. 8. On the left, the raw beam outside the chest and the catheter inside the heart are clearly detected. Pulmonary vasculature and the inferior vena cava are clearly visible within the chest. The

ig. 8

limited number of angles of view, the effect of x-ray scatter and the mechanical imprecision of the rotation of the dog in front of the imaging chain results in a true spatial and density resolutions of 6 mm and 10%, respectively, within the cross section. Contrast medium-filled coronary arteries of less than 1 mm diameter can be visualized in the intact heart when the image isocon is operated so that those regions of the image with low information content (raw beam and chest wall) are over the "knee" of the characteristic brightness/signal output curve of the camera, scattered radiation is reduced by collimination of the incident and transmitted x-rays to a fan beam and a focused colliminator oriented at right angles to the plane of this fan beam is used.

DISCUSSION

This prototype x-ray imaging system has been shown to be adequate for three-dimensional cross-sectional reconstruction of the intact thorax and its contents. The anatomic shape and dimensions of the lungs and epicardial surfaces can be imaged without the use of intravascular agents. These 60-per-second images can be viewed in real time or stop-action for quantitative analysis of pulmonary function and provide qualitative information as to cardiac malformations and abnormal dynamics. Simultaneous visualization of

the epi- and endocardial surfaces of the heart at 60 images/second can be achieved, if at least 10% concentration of iodinated roentgen contrast medium is present in the blood stream. Reconstruction of the epicardial and endocardial surface will permit quantitative analysis of cardiac anatomy and function. In addition, the presence of 50% concentration contrast medium in smaller vessels such as the coronary arteries will permit quantitative analysis the three-dimensional anatomy and segmented flow through the coronary macrovasculature and regional myocardial perfusion. Detection of disease processes which perturb the anatomic structure or function of the circulatory system in any region of the body will also be possible.

Use of this prototype imaging chain in a reconstruction (computerized tomography) system is a compromise between speed of data acquisition (i.e., temporal resolution) and spatial-density resolution. Future modifications of the system should be aimed at increasing the efficiency of the imaging chain and reduction of degradation of the image due to x-ray scatter and other efforts to increase the signal-to-noise ratio of the overall system. Improvement of the x-ray focused grid and fluorescent screen are especially required.

ACKNOWLEDGEMENTS

The authors would like to thank especially Messrs. Merrill Wondrow, Don Erdman, Julijs Zarins, Donald Hegland, Chris Hansen and

Ronald Roessler who provided invaluable assistance with the design, fabrication and experiments, and Ms. Pat Snider and Ms. Donna Balow and their colleagues for their assistance with typing and illustrations.

REFERENCES

Berggren, M. J., S. A. Johnson, J. F. Greenleaf, R. A. Robb, R. E. Sturm, G. T. Herman, and E. H. Wood: A method for selective tissue and chemical element three-dimensional reconstruction imaging from radiographic film and roentgen-video images. Image Processing for 2-D and 3-D Reconstruction from Projections: Theory and Practice in Medicine and the Physical Sciences. A Digest of Technical Papers, August 4-7, 1975, Stanford, California, pp MB2-1 - MB2-4

Gilbert, B. K., M. T. Storma, C. E. James, L. W. Hobrock, E. S. Yang, K. C. Ballard, and E. H. Wood: A real-time hardware system for digital processing of wideband video images. IEEE Transactions on Computers (in press)

Heintzen, P. and K. Moldenhauer: The x-ray absorption by contrast material: Theoretical consideration. In: Roentgen, Cine, and Videodensitometry: Fundamentals and Applications for Blood Flow and Heart Volume Determination, pp 73-81, ed. by P. Heintzen, George Theim Verlag Stuttgart 1971

Johnson, S. A., R. A. Robb, J. F. Greenleaf, E. L. Ritman, S. L. Lee, G. T. Herman, R. E. Sturm, and E. H. Wood: The problem of accurate measurement of left ventricular shape and dimensions from multiplane roentgenographic data. Eur. J. Cardiol. 1/3:241-258 (1974)

RCA Electro-Optics Handbook. Commercial Engineering, Harrison Nj07029 (2nd ed.) 1974

Ritman, E. L., S. A. Johnson, R. E. Sturm, and E. H. Wood: The television camera in dynamic videoangiography. Radiology 107:417-427 (1973)

Ritman, E. L., R. E. Sturm, and E. H. Wood: Needs, performance requirements and proposed design of spatial reconstruction system for diagnostic and investigative studies of cardiopulmonary and circulatory dynamics. In: Reconstruction Tomography in Diagnostic Radiology and Nuclear Medicine, edited by M. E. Phelps, G. L. Brownell, G. R. Cox, Jr., D. O. Davis, R. G. Evens, Baltimore, University Park Press, 1976 (in press)

Robb, R. A., S. A. Johnson, J. F. Greenleaf, M. A. Wondrow, and E. H. Wood: An operator interactive computer controlled system for high fidelity digitization and analysis of biomedical images. Proc. Soc. Photo-Optical Inst. Eng. 40:11-26 (August 27-29, 1973)

Robb, R. A., E. L. Ritman, J. F. Greenleaf, R. E. Sturm, G. T. Herman, P. A. Chevalier, H. K. Liu, and E. H. Wood: Quantitative imaging of dynamic structure and function of the heart, lungs and circulation by computerized reconstruction and subtraction techniques. Presented at the Proceedings of the Third Annual Conference on Computer Graphics (SIGGRAPH), Philadelphia, Pennsylvania, July 14, 1976 (in press)

Robb, R. A., E. H. Wood, E. L. Ritman, S. A. Johnson, R. E. Sturm, J. F. Greenleaf, B. K. Gilbert, and P. A. Chevalier: Three-dimensional reconstruction and display of the working canine heart and lungs by multiplanar x-ray scanning videodensitometry. Proceedings of the Computers in Cardiology Conference IEEE Computer Society, Bethesda, Maryland (October, 1974) pp 151-163

Robinson, A. L.: Image reconstruction (I): Computerized x-ray scanners. Science 190:542-543;593, November 7, 1975

Robinson, A. L.: Image reconstruction (II): Computerized scanner explosion. Science 190:647-648, November 14, 1975

Sturm, R. E. and R. M. Morgan: Screen intensification systems and their limitations. Am. J. Roentgenol. Radium Ther. 62:617-634 (1949)

AD-A038 014 MAYO FOUNDATION ROCHESTER MINN DEPT OF PHYSIOLOGY AN--ETC F/G 6/19
PROTECTION OF THE CARDIOPULMONARY SYSTEMS AGAINST THE INJURIOUS--ETC(U)
AUG 76 E H WOOD, P A CHEVALIER F44620-71-C-0069

UNCLASSIFIED AFOSR-TR-77-0316 NL

2 OF 2
AD
AD38014

END
DATE FILMED
4-77

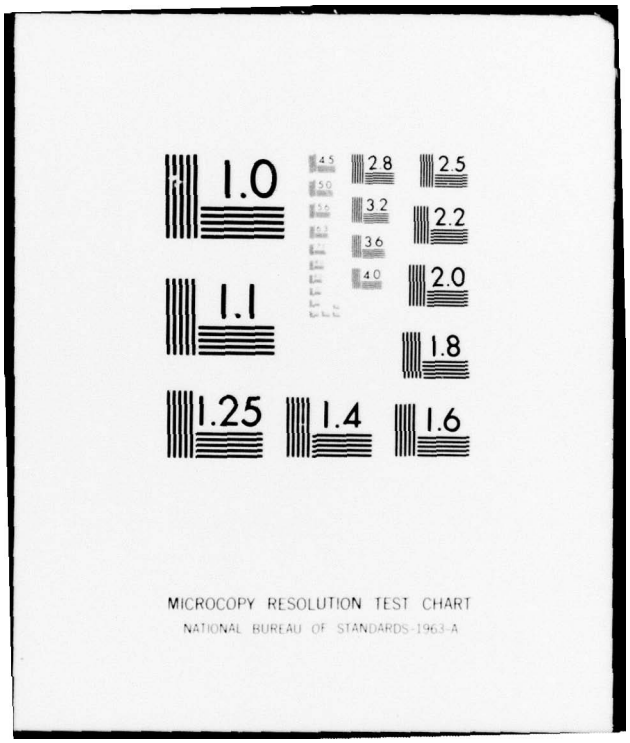
1.0
1.1
1.25
1.4
1.6
1.8
2.0
2.2
2.5
2.8
3.2
3.6
4.0
4.5
5.0
5.6
MICROCOPY RESOLUTION TEST CHART
NATIONAL BUREAU OF STANDARDS-1963-A

LEGENDS

Fig. 1 Schematic arrangement of a single roentgen video imaging chain for high temporal resolution computerized tomography, a dynamic spatial reconstruction system. The intensity of each x-ray pulse, every 1/60 second, is monitored by the ionization chamber so as to provide a value proportional to radiation incident on the subject under study (see text for details). (Cardiovascular Imaging and Processing. Theory and Practice. Soc. Photo-Optical Inst. Eng. 72:103-122 (1975))

Fig. 2 Efficiency of imaging chain depicted by tracing x-ray photons through system. A theoretical relationship of the signal-to-noise of this type of imaging chain has been derived and is expressed by the equation for S/N. This equation gives a theoretical signal-to-noise ratio of 35/1 in the thickest part of the chest (i.e., where greatest x-ray absorption occurs) (see text for details). (Proceedings of the San Diego Biomedical Symposium, February 4-6, 1976, San Diego, California, in press)

Fig. 3 Signal noise in the SSDSR imaging chain was measured as four standard deviations of the sample-to-sample variation of the voltage of the video signal about the mean value measured at the same site (i.e., pixel) on a single video line. Panel (a) - the intensity of the highly collimated x-ray beam was attenuated by

placing 10 and 20 cm water between the x-ray source and fluorescent screen while KV and ma of the x-ray system were left unchanged. The dashed curve was calculated on the theoretical basis that the noise in the video signal should be proportional the square root of the magnitude of this signal. The magnitude of the calculated noise was assumed to be identical to the measured noise at the 700 mv signal level. The measured noise falls less rapidly than the calculated values indicating that noise, over and above that to be expected from the x-ray image, contributes to the imaging chain signal noise.

Panel (b) - The measured signal noise (solid lines) decreased similarly to the calculated (dashed lines) when an increasing number of signal samples were averaged. The calculated and measured values are for a video signal level of 700 mv measured at the same site on the same video line (i.e., the same pixel) at successive 30/sec instants in time (curve I). The measured decrease in noise is virtually identical to the calculated values, indicating that the noise is statistical in nature. When the video signal values were measured at the same site on different successive video lines, i.e., from the same vertical column of A/D samples, in one image, the statistical nature of the noise was also confirmed (curve II). Curve III is based on values obtained by averaging signal samples along the same horizontal video line in the same uniform gray level image. This curve indicates that there is a non-statistical bias in the noise (possibly caused by variations in the structure

bias in the noise (possibly caused by variations in the structure of the image or signal induced oscillations in the electronic circuitry.

Fig. 4 Schematic of assembly to provide programmable computer control of the sweep (read-off) frequency of a video camera. Because of the integrating characteristics of the input imaging target of the camera, when high temporal resolution is not required, its sensitivity to low light levels can be increased by decreasing the sweep frequency from the normal 30 or 60-per-second value to 1-per-second or less (see Fig. 7).

Fig. 5 a. Photo of x-ray image of test grid consisting of crossed radiopaque wires 2 cm apart, and cross hatchings 2 mm apart along the central cross wires. The slight barrel distortion in this photograph is primarily due to the videomonitor because the horizontal wires remain in alignment with the horizontal video lines.

b. Photo of x-ray image obtained of a step-wedge containing 1, 8 15, 22, and 29 layers (each 0.63 cm thick) of pressed wood using 120 kv peak x-ray beam pulsed 60-per-second, each pulse 0.34 msec duration. Two steel wires 0.5 and 1.0 mm diameter were strung diagonally across the wedge. In this system, 10% of the incident x-ray beam was transmitted through 18 layers of pressed wood as

measured at the fluorescent screen with a Victoreen radiation meter. The video signal deflection (panel d) caused by the 1 mm steel wire is clearly distinguishable in the video signal corresponding to the 22 layers of pressed wood. Direct observation of the x-ray image on the videomonitor permits clear visualization of the 1.0 mm wire through the 29 layers of pressed wood.

c. The video signal of a single horizontal video line near the middle of the roentgen video image in panel a is displayed to illustrate the radial fall-off in image brightness. The amplitude of the signal above zero is directly proportional to image brightness and the square wave deflections on the far left and right are video synchronization signals. Most of the fall-off is attributable to the optical system and the operational characteristics of the image isocon.

d. The video signal of a single horizontal video line near the middle of the roentgen video image in panel b is displayed to illustrate the decrease in video signal noise (thickness of trace) with decrease in signal magnitude. The peak-to-peak noise in the video image is approximately 10% of peak signal ("raw" beam) and 1% over the 29 layers of pressed wood where the signal is about 1% of "raw" beam. The deflections caused by the steel wires are visible in the signal corresponding to the x-ray transmitted through the 22 and 15 layers of pressed wood for the 1 mm and 0.5 mm steel wires,

respectively. (Proceedings of the San Diego Biomedical Symposium, February 4-6, 1976, San Diego, California)

Fig. 6 Increasing depth of water transradiated by 100 kv x-ray beam results in exponential decrease in video signal as shown in curve I. At increasing depths, the decrease of video signal becomes less rapid due to "hardening" of the remaining x-ray beam. The relationships in curve II were obtained by increasing the x-ray beam intensity so that the signal from the x-ray beam attenuated by less than 5 cm of water exceeded the linear segment (the "knee") of response curve of the image isocon camera.

Fig. 7 Integration of successive pulsed x-ray images on the image isocon tube target results in a linear increase in the video signal amplitude when this is "read" out after completion of the integration period. To prevent non-linear integration at very low image intensities, the periphery of the x-ray image was highly illuminated during the integration period so as to maintain proper target potential. The noise in the imaging system remains proportional to the video signal (see Figure 3a) so that a ten-fold increase in signal from 70 mv to 700 mv results in an increase in noise of approximately six-fold (theoretically approximately three-fold) so that a two-fold increase of signal noise results in addition to the ten-fold (more than 3 bit) increase in analog-to-digital conversion resolution in that part of the image of interest.

Fig. 8 Left panel: Monoplane lateral roentgen projection image of dog thorax. The brightened line indicates the level of the reconstructed cross section shown in right panel.

Right panel: Cross-sectional image was computed from roentgen density profiles measured from same horizontal video line recorded at 28 equispaced angles of view around an arc of 160°. Similar cross-sectional images can be computed from each of the 240 horizontal video lines contained in each 60-per-second video field image. Physiologic stationarity of the respiratory and cardiac cycles plus synchronization with the x-ray pulsing and video recording cycles are required for accurate reconstruction of the thorax of intact anesthetized dogs when a single roentgen-video image chain and consequent mandatory mechanical circumferential scanning are used (R. E. Sturm, et al., Proceedings of the San Diego Biomedical Symposium, February 4-6, 1976, San Diego, California, in press)

IMAGING CHAIN SSDSR

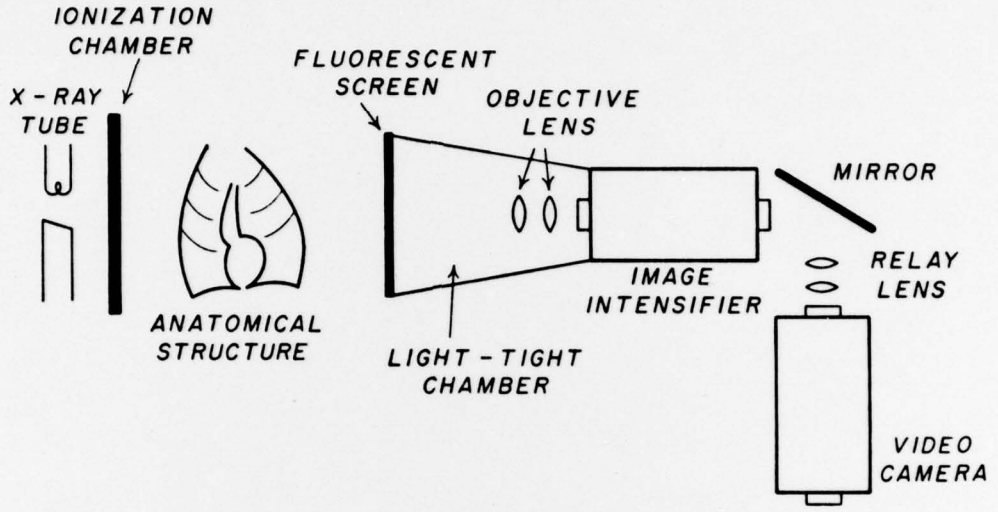

Fig. 1

SIGNAL-TO-NOISE RATIO OF DSR IMAGING CHAIN

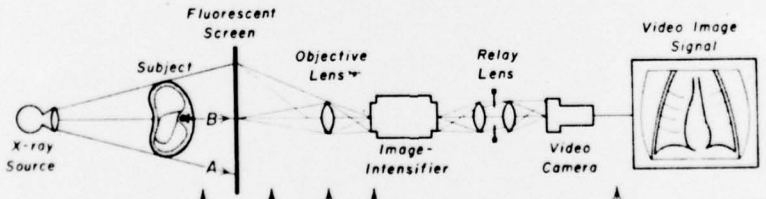

B - Through Chest
A - Unattenuated Beam

$$S/N = \sqrt{\frac{n}{1+1/qmE}}$$

n m E q S,N

S,N = VIDEO SIGNAL SIGNAL/NOISE

	X-RAY PHOTONS/mm² of FLUORESCENT SCREEN/EXP^R A	B
1.4 PHOTOELECTRONS/X-RAY PHOTON ABSORBED (11% Efficiency of Photocathode)	2.4×10^5	2.4×10^3
13.5 LIGHT PHOTONS/X-RAY PHOTON ABSORBED (2.7×10^{-3} Efficiency of Lens)	2.2×10^6	2.2×10^4
5,000 LIGHT PHOTONS/X-RAY PHOTON ABSORBED (50% of Light Photons Produced by X-Ray Photons are Useful)	8.3×10^8	8.3×10^6
1 X-RAY PHOTON ABSORBED by SCREEN	1.7×10^5	1.7×10^3
2 X-RAY PHOTONS (Normalized to 70 kv) INCIDENT on SCREEN	3.3×10^5	3.3×10^3

Fig. 2

SIGNAL / NOISE OF SSDSR
Effect of Signal Averaging
(Signal 700 mv, 2 MHz Band Width)

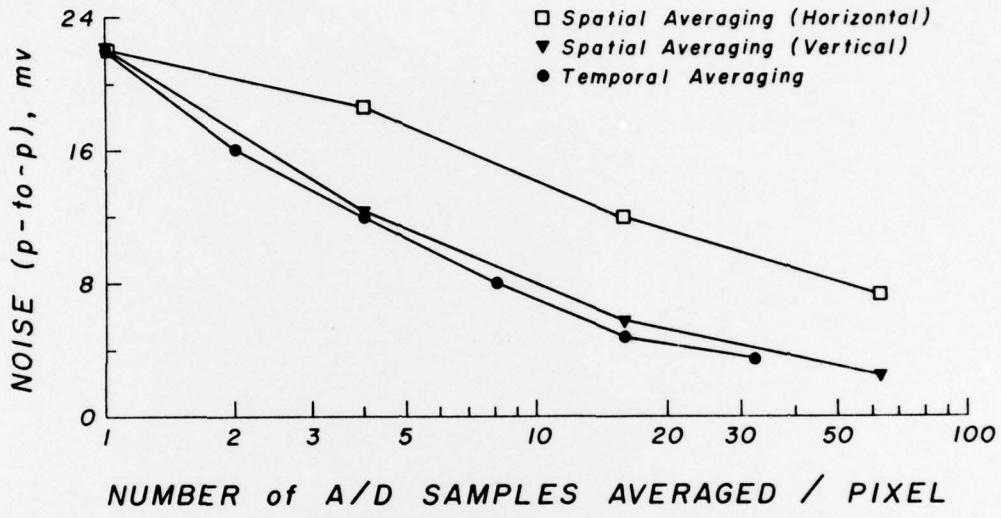

Fig. 3

SINGLE-SOURCE DYNAMIC SPATIAL RECONSTRUCTOR IMAGING SYSTEM
Computer-Controlled Video-Camera Integration and Recording for Low-Intensity Radiation Imaging

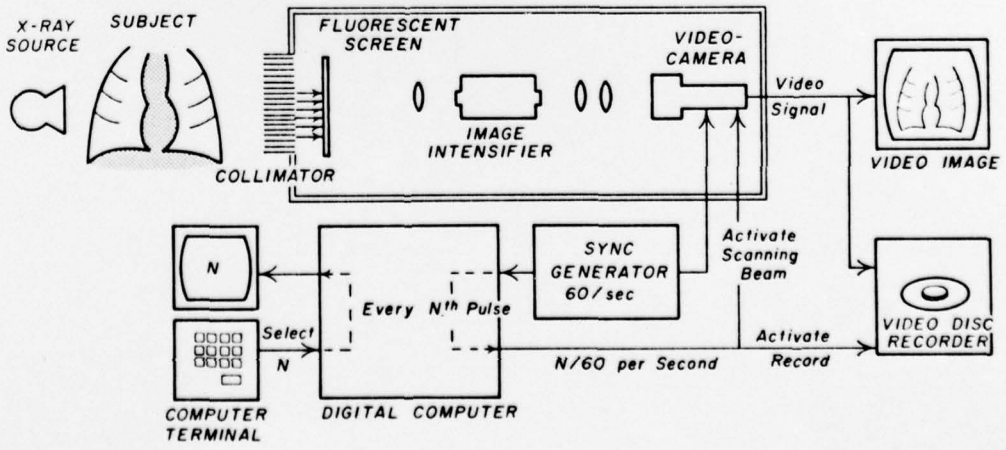

Fig. 4

IMAGING CHARACTERISTICS OF SSDSR

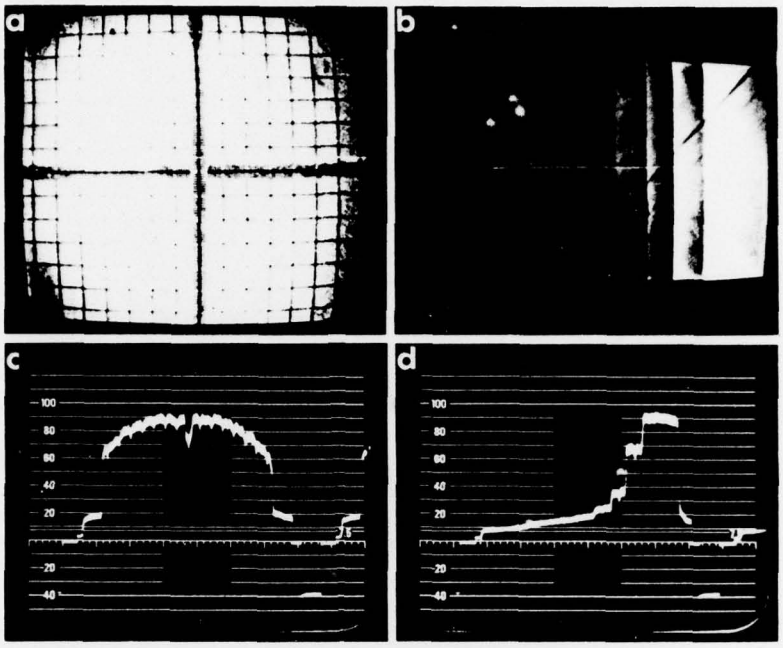

Fig. 5

SSDSR – X-RAY INTENSITY INPUT/ VIDEO SIGNAL OUTPUT RELATIONSHIP

100 kv, 4 ma, Gd_2O_2S: Tb Screen

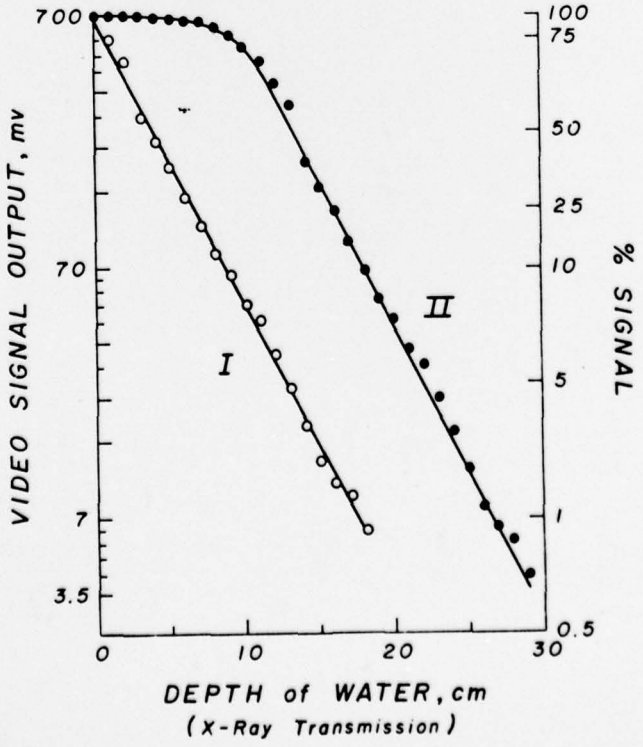

Fig. 6

SINGLE-SOURCE DYNAMIC SPATIAL
RECONSTRUCTOR IMAGING CHAIN
Integration Time / Gain Relationship
(100 kv, 60 pulses / second)

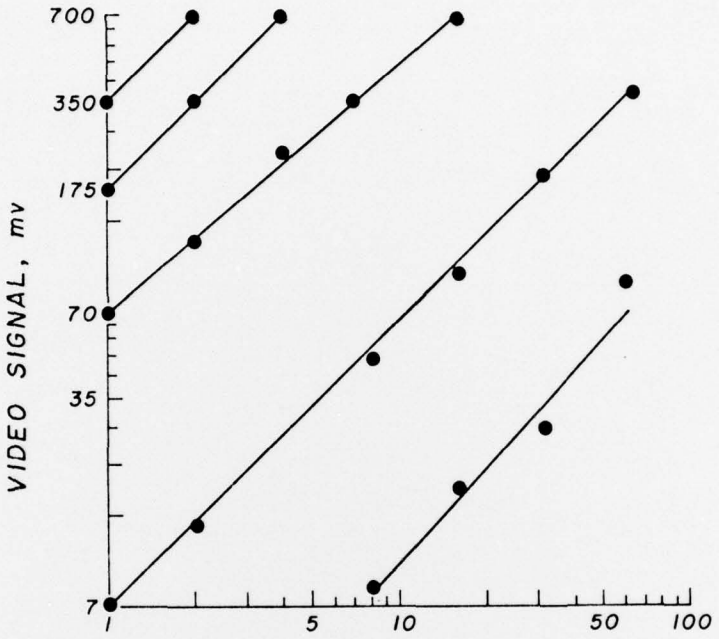

Fig. 7

RECONSTRUCTED CROSS SECTION OF DEAD DOG THORAX

Projection at 180° Central Cross Section

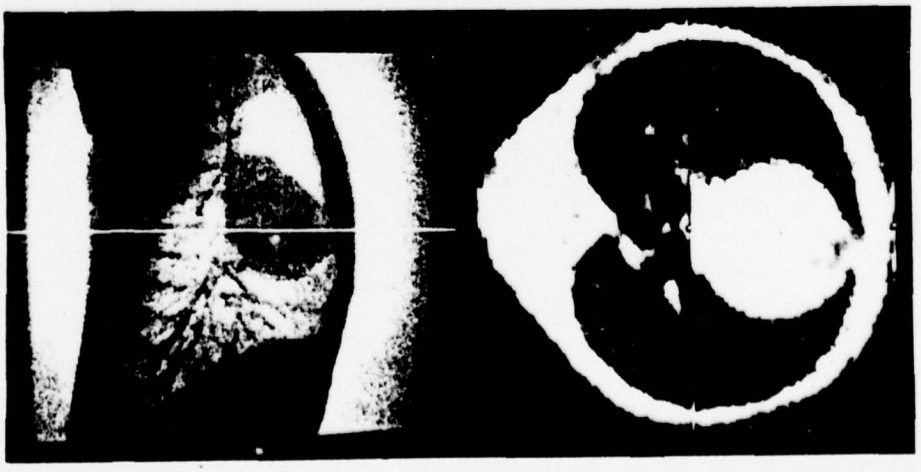

Fig. 8